A UNITED STATES DEPARTMENT OF COMMERCE PUBLICATION

NOAA Technical Memorandum NESS 52

U.S. DEPARTMENT OF COMMERCE
National Oceanic and Atmospheric Administration
National Environmental Satellite Service

Operational Products From ITOS Scanning Radiometer Data

EDWARD F. CONLAN, Compiler

WASHINGTON, D.C.
October 1973

NOAA TECHNICAL MEMORANDA

National Environmental Satellite Service Series

The National Environmental Satellite Service (NESS) is responsible for the establishment and operation of the National Operational Meteorological Satellite System and of the environmental satellite systems of NOAA. The three principal offices of NESS are Operations, Systems Engineering, and Research.

NOAA Technical Memoranda NESS series facilitate rapid distribution of material that may be preliminary in nature and may be published formally elsewhere at a later date. Publications 1 through 20 and 22 through 25 are in the former series, ESSA Technical Memoranda, National Environmental Satellite Center Technical Memoranda (NESCTM). The current series, NOAA Technical Memoranda, National Environmental Satellite Service (NESS), includes 21, 26, and subsequent issuances.

Publications listed below are available from the National Technical Information Service, U.S. Department of Commerce, Sills Bldg., 5285 Port Royal Road, Springfield, Va. 22151. Price: $3.00 paper copy; $1.45 microfiche. Order by accession number, when given, in parentheses.

ESSA Technical Memoranda

NESCTM 15 Some Aspects of the Vorticity Structure Associated With Extratropical Cloud Systems. Harold J. Brodrick, Jr., May 1969. (PB-184-178)

NESCTM 16 The Improvement of Clear Column Radiance Determination With a Supplementary 3.8μ Window Channel. William L. Smith, July 1969. (PB-185-065)

NESCTM 17 Vidicon Data Limitations. Arthur Schwalb and James Gross, June 1969. (PB-185-966)

NESCTM 18 On the Statistical Relation Between Geopotential Height and Temperature-Pressure Profiles. W. L. Smith and S. Fritz, November 1969. (PB-189-276)

NESCTM 19 Applications of Environmental Satellite Data to Oceanography and Hydrology. E. Paul McClain, January 1970. (PB-190-652)

NESCTM 20 Mapping of Geostationary Satellite Pictures--An Operational Experiment. R. C. Doolittle, C. L. Bristor, and L. Lauritson, March 1970. (PB-191-189)

NESCTM 22 Publications and Final Reports on Contracts and Grants, 1969--NESC. January 1970. (PB-190-632)

NESCTM 23 Estimating Mean Relative Humidity From the Surface to 500 Millibars by Use of Satellite Pictures. Frank J. Smigielski and Lee M. Mace, March 1970. (PB-191-741)

NESCTM 24 Operational Brightness Normalization of ATS-1 Cloud Pictures. V. R. Taylor, August 1970. (PB-194-638)

NESCTM 25 Aircraft Microwave Measurements of the Arctic Ice Pack. Alan E. Strong and Michael H. Fleming, August 1970. (PB-194-588)

NOAA Technical Memoranda

NESS 21 Geostationary Satellite Position and Attitude Determination Using Picture Landmarks. William J. Dambeck, August 1972. (COM-72-10916)

NESS 26 Potential of Satellite Microwave Sensing for Hydrology and Oceanography Measurements. John C. Alishouse, Donald R. Baker, E. Paul McClain, and Harold W. Yates, March 1971. (COM-71-00544)

NESS 27 A Review of Passive Microwave Remote Sensing. James J. Whalen, March 1971. (COM-72-10546)

NESS 28 Calculation of Clear-Column Radiances Using Airborne Infrared Temperature Profile Radiometer Measurements Over Partly Cloudy Areas. William L. Smith, March 1971. (COM-71-00556)

(Continued on inside back cover)

U.S. DEPARTMENT OF COMMERCE
National Oceanic and Atmospheric Administration
National Environmental Satellite Service

NOAA Technical Memorandum NESS 52

OPERATIONAL PRODUCTS FROM ITOS SCANNING RADIOMETER DATA

Edward F. Conlan,
Compiler

Data Processing and Analysis Division

WASHINGTON, D.C.
October 1973

UDC 551.507.362.2:551.508.21:551.506ITOS

551.5	Meteorology
.506	Observational data
.507.362.2	Meteorological satellites
.508	Instruments
.21	Radiometers
ITOS	Improved TIROS Operational Spacecraft

CONTENTS

OPERATIONAL PRODUCTS AVAILABLE THROUGH DIGITAL PROCESSING OF ITOS SCANNING RADIOMETER DATA

Edward F. Conlan, Compiler
National Environmental Satellite Service, NOAA, Washington, D.C.

ABSTRACT. This report is intended as a manual for the potential user of processed data obtained from the ITOS scanning radiometers. Major contributions have been made by experts involved in the various processing phases. The intent has been to convey primary information in the main text so as to provide an overview for the customer whether his mission be oriented toward operations or research. With this in mind, an attempt is made to minimize the use of specialized phraseology. It is to be expected that a potential user may thereby assess the potential value of the information for his mission even though his familiarity with spacecraft operations or automatic data processing may be limited. Specifically, he may gain insight as to earth location accuracy, precision and stability of calibrated data, areal extent, and timewise availability of products.

1. DATA SOURCE

A. The Spacecraft and Scanner System

TIROS M, the prototype Improved TIROS Operational Spacecraft (ITOS 1), was launched on January 23, 1970; the second spacecraft in the series, NOAA 1, was placed in orbit on December 11, 1970. Both satellites were certified by NASA and turned over to the National Environmental Satellite Service (NESS) for operational use. The latest in the series, NOAA 2, was launched October 15, 1972.

Since a description of the spacecraft is available elsewhere, only a few pertinent details will be mentioned here (Schwalb, 1972). The 741-lb rectangular sensor box is spin stabilized with a counter-revolving momentum flywheel so that the box rotates once per orbital period. With the spin axis perpendicular to the orbital plane, and pitch sensors providing relative speed control between flywheel and satellite, the resulting earth oriented platform provides for the mounting of scanning radiometer (SR) imaging sensors. Attitude control is accomplished by coils that provide magnetic torqueing.

The NOAA 2 spacecraft is in a nominal 790-n mi orbit having a 117-min period. A 78° retrograde inclination provides sun synchronism with equator crossings near 0850 southbound and 2050 northbound local solar time.

Since the SR is a two-channel device (0.52- to 0.72-μm visible and 10.4- to 12.5-μm infrared), there is opportunity for three global imagings each day, one in the visible and two in the infrared. Resolution near the subpoint is nominally 4 mi for the IR channel and 2 mi for the visible channel. This resolution, combined with the instrument scan rate and forward motion, results in contiguous scan lines in the IR channel, but 2-n mi gaps in the visible scan at subpoint. With two such scanner units and redundant tape recorder facility, the SR is the prime imagery sensor aboard the spacecraft; as such, it replaces the vidicon cameras which have been a part of all spacecraft in the TIROS series prior to NOAA 2. Further details of the SR package are provided by Schwalb (1972).

B. Data Acquisition and Relay

Through guidance received from the Spacecraft Operational Control Center (SOCC) at Suitland, Md., the SR data are acquired at the NESS Wallops Island, Va., or the Gilmore Creek, Alaska, Command and Data Acquisition (CDA) facilities. On command, the contents of the SR tape recorders are transmitted to the CDA as an FM signal. Information recorded over the entire orbital period is read out at high speed so that the acquisition cycle takes place in about 5 min. Scan data sensed during tape readout are stored on the alternate recorder with acquisition delayed until a later readout cycle. The visible and infrared data are combined into a single data stream that also contains appropriate synchronization and telemetry data. A single tape recorder track is used for onboard storage between readout cycles of this time-multiplexed data.

A direct readout capability is also provided so that the worldwide assemblage of Automatic Picture Transmission (APT) stations, with some hardware modifications, may receive scanner image data. This AM signal may also be acquired at the CDA stations as a supplement to the stored data.

All SR data received at the CDA stations are relayed to Suitland via broadband microwave communication links. The relayed signal remains in analog form and is relayed at one-fourth of the speed at which it is acquired. Ground-based analog tape recording facilities at the CDA stations provide the means for the data relay slowdown. When problems develop, the same equipment makes possible the retransmission of data.

2. RAW DATA INGESTION

As the raw scanner signals arrive at Suitland, the on-line processing is carried out by a Digital Data Handling System (DDHS). A manuscript report (Kahwajy 1970) describes the discrimination, synchronizing, digitizing, and formatting functions of this computer-based facility. Additional analog tape buffering options are provided at the input to this system.

In the case of incoming SR signals, the active portion of the system corrects for tape recorder flutter and wow to ensure a uniform digital sampling rate. A fixed pattern "sync pulse" injected into the signal as a function of scan shaft phase angle is detected to synchronize (and maintain coherency of)

earth scan data. Housekeeping telemetry frame synchronization is also carried out to separate "back scan" data from earth imaging information.

Figure 1 shows the component signals contained in a single 360° sweep of time-multiplexed data. Proceeding along the scan from left to right, the low signal portion of the sync pulse provides a presynchronizing warning. At this point the computer sets up the desired sampling rate in the sample rate controller, and as the sharp sync rise is encountered, true synchronizing takes place. At this precise moment, the digitizer starts producing 8-bit samples at the prescribed rate. Following the porch pattern, the SR processor inserts telemetry information in the SR data stream, after which the sensor responds to a sun shield followed by a brief measure of space response. A sharp warming in the IR data is then indicated as the earth scan begins. After the variable earth scene response, a sharp cooling is observed at the off-going horizon. Following this, visible channel data are multiplexed into the data stream. The visible data are in a format comparable to the IR data (fig. 1). After the visible channel data are multiplexed, the entire cycle repeats itself.

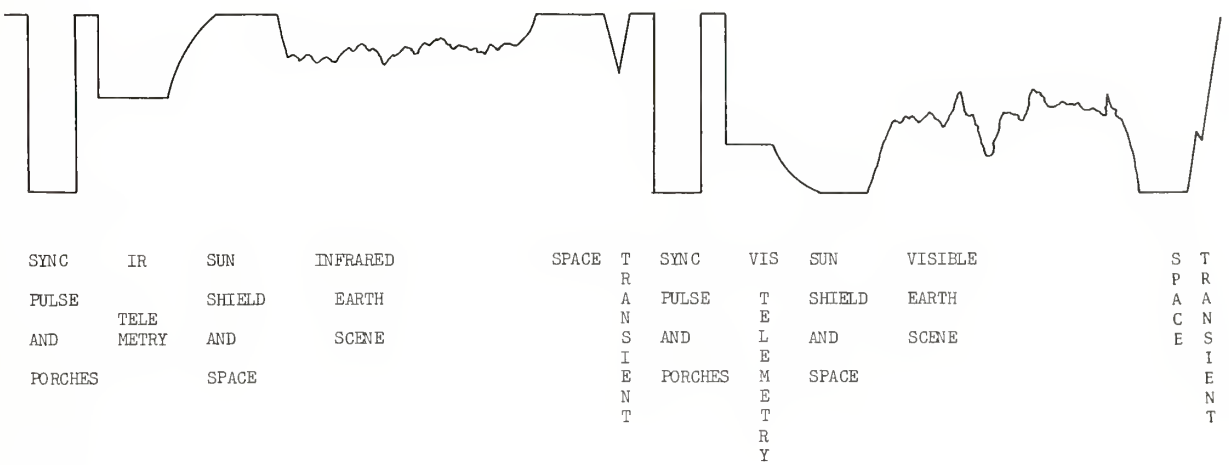

Figure 1.--*Scanning radiometer data format*

During the telemetry channel periods a step wedge (used in normalizing the raw count range in conformity with known signal voltages) is inserted in the data stream for 14 of each 25 lines. Other spin cycles include alternate information on the back scan until a sequence of 25 items is measured. One of the items included is relative time measured to quarter-second precision by the spacecraft clock. It is thus convenient to consider a 25-scan-line data "frame" as an integral unit, since all information for eventual quantitative use is contained in such a sequence. Further details concerning items in each multiplexed data frame are available in the technical literature (RCA). Other details concerning extraction of needed housekeeping data and signal quality diagnoses are available only as manuscript computer program notes and other software documentation.

Digital sampling rates are based upon considerations of natural scene and spatial frequencies detected by the sensor and passed by the communications

system. Modulation Transfer Function (MTF) curves have been derived by the sensor manufacturer (Feniger 1969). For those using the raw ingest data tapes, further information on formats and sampling rates, for both stored and directly transmitted SR data, is provided in appendix A.

3. PREPROCESSING AND SIGNAL CONDITIONING

Once the raw ingest data are available on tape, the computation steps and extraction of quantitative information can begin. The first step involves the "electrical normalization" of raw counts to insure strict correspondence with the prescribed signal voltage range. Prelaunch bench checks yield such count-to-volt curves for each sensor system. However, the voltage range obtained from the incoming analog signal involves detector adjustments (frequency limit settings in the case of the FM discriminator for recorded SR, and amplitude adjustment of the demodulator used for the detection of direct readout scanner data). The step wedge contained in the backscan for each 25-sweep data frame is used for the normalization. Analysis of the digital counts samples for each of the wedge steps results in the generation of a table for transforming all raw counts into proper equivalent values as specified in the prelaunch checks. So long as equipment misadjustment does not cause saturation ("clipping") at either extremity of the response range, this normalizing procedure will ensure meaningful count values.

The next step involves the calibration of the radiometer response in terms of voltage versus temperature or brightness.

Prelaunch calibration by the vendor has provided the voltage-to-temperature (or brightness) response relation for each sensor system (Feniger 1969). The program provides families of lookup tables for each sensor for converting normalized raw counts into effective blackbody radiative temperature responses (IR), or into calibrated brightness response for the visual channel. These values are then corrected for any bias as a function of sensor temperature--a measurement regularly available in the telemetry data.

The final step involves corrections necessary for the interpretation of measurements of the natural earth scene. In the case of the IR sensor, corrections must be made for atmospheric attenuation. Smith et al. (1970) provided an algorithm that specifies this "limb darkening" correction as a function of local zenith angle, with the assumption that water vapor is the primary absorbing constituent.

For the visual channel, final correction of the brightness response is made as compensation for differences in solar illumination of the earth scene. After due consideration of the more sophisticated "3-angle" approach (Ruff et al. 1966), a more basic beginning approach was adopted. This algorithm is a simple, cosine function of the solar zenith angle; previously, a less satisfactory model was tried using weighting functions generated empirically from NOAA 1 data with an approach previously applied to geostationary satellite image data (Taylor 1970). Research is now underway to develop a viable three-angle model. Further details on calibration, limb darkening, etc., are contained in appendix B.

4. EARTH LOCATION

Implicit in the procedures for correcting limb darkening and normalizing brightness is the need for position information. A companion to these correction activities is therefore the task of relating each digitized response sample to the earth scene. The various inputs and the approach have been described earlier (Bristor 1970). Items required for this task, together with brief explanatory remarks, are summarized in the following paragraphs:

a. Spacecraft position: Basic orbital elements for the ITOS spacecraft are provided by NASA through the acquisition of tracking information and the combining of these data with a rather sophisticated orbital model. The orbital elements are then available for use with a prediction program that provides satellite location as a function of time.

b. Scanner mounting: The scan sweep must be oriented with respect to the spacecraft; this is determined prior to launch by the mounting and alinement checks. In addition, the instantaneous position of the mirror within the scan shaft spin phase cycle is required. Accordingly, the porch response is injected into the signal path at a prescribed angle between the scan shaft and the spacecraft base plate.

c. Angular increment: Knowledge of the angular increment through which the scan shaft turns between adjacent digital response samples is required for the proper spacing deployment of samples across the earth scan sweep. This, in turn, requires precise knowledge of shaft spin rate and digital sampling rate.

d. Horizon location: Each scan sweep sample population must additionally be deployed in synchronism with the earth disk. With the present approach, horizon detection logic is used to detect both limbs of the earth disk.

e. Attitude: Although earth oriented, the ITOS sensor platform is a spin stabilized vehicle. With knowledge of 2, 3, and 4 above, the SR data are used to obtain the right ascension and declination of the spin vector following procedures developed by R. Doolittle and H. Sparks of NESS. In brief, the roll/yaw components of this vector are determined by obtaining the angle between earth horizon and porch through a count of the intervening sample population on each scan sweep. The pitch component is expressed as an error signal between the observed position of horizon pitch pulses and their predicted position as specified in the feedback control mechanism.

f. Time: Time is the linkage by which scan sweeps are related to orbital positions. A 24-bit quarter-second interval counter is used on the spacecraft for this purpose, and its output is reported during backscan within each data frame. This relative time is then related to absolute time as the counter reset command is issued at the CDA station.

With the above inputs, the earth location process can be carried out, since the orientation of the sensing beam is known with respect to a platform whose position and orientation with respect to the earth are also known at all times. To reduce computation penalty, the earth location linkage is provided by means

of an open lattice of image points. A similar process for earth location of vidicon imagery was described earlier (Bristor et al. 1966). Briefly, the three-dimensional image location element vector, available at the spacecraft, is converted to an equivalent geocentric vector through coordinate transformation equations to obtain an earth's surface latitude-longitude location for the sample. Since the original image perspective must be transformed to some standard map projection, the computed location is transformed to an equivalent location on the desired projection. For convenience, map coordinates are expressed in terms of a fine-mesh, square overlay grid, suitably oriented and scaled to approximate the basic resolution of a sensor sample element. The computer logic is further simplified by using scanner line number and sample number intervals in binary steps for the open lattice calculations. The resulting "bench point" calculations for the SR data are made for every eighth line and 32nd sample. See appendix D for a comprehensive discussion of the procedures.

In terms of computational efficiency, this image mapping input has drawbacks. With greatly overlapped raw data samples, an obvious population surplus exists if the mapping process merely replots samples into a nonoverlapped square mesh map array. In addition, a square mesh overlay on a map, which is not an equal area projection, cannot uniformly equate mesh size to basic sensor sampling resolution. The result is that several input data samples may compete for map mesh locations in certain portions of the map. (A square mesh sector on a polar stereographic map encompasses four times the acreage at the pole as does a similar square near the equator.) An alternate approach (Roth 1969) starts with the map mesh coordinates and computes the input data scan line and sample number for the input sample most eligible for mapping into that location. Thus, only the desired input samples are unpacked and replotted. Because of evolutionary software investments, the first method described above has been retained, but with changes aimed at minimizing the mentioned penalties.

5. MAPPING AND GRIDDING

With orthogonal bench point earth locator inputs, SR data are mapped daily over the entire globe in polar stereographic format. A tropical belt covering the full 360° longitudinal span is redundantly mapped in Mercator format. Several sections are also mapped with finer mesh to retain the maximum input sample volume for special applications.

The mapping algorithm may be summarized in the following steps:

a. A bench point earth locator array is computed and the limits of the equivalent fine mesh map array are calculated.

b. The specified sector of the map image array is transferred from dedicated disk storage into main computer memory.

c. Calibrated input scan data potentially available for mapping are read into main memory.

d. Using scan line and sample number designators, the location in the

map array for a sample is computed from the bench point array. Taking advantage of a rectangular binary population organization, a linear interpolation is accomplished entirely by binary shift logic without need for more costly multiply instructions.

e. Candidate samples are replotted in the map mesh array until input sampling is exhausted, or until the map array and bench point fields are exhausted.

f. The resulting mapped imagery is replaced in disk memory where it becomes available as a source for display and for other more quantitative information extraction operations.

A. Global Polar Mosaics

As in mapping vidicon camera data (Bristor et al. 1966), the fine mesh polar stereographic arrays have been aligned with the conventional Numerical Weather Prediction (NWP) grid so derived products may be conveniently adapted to that application. By subdividing each coarse mesh length into 32 segments, one obtains a 2048 x 2048 array with a 4-mi mesh size near the equator. Unfortunately, the map distortion factor doubles this mesh length distance at the pole. Two such arrays provide global coverage (see figs. 2a, b, c, d, e, and f).

With a 2048 x 4096 vertical rectangle formed by placing the Northern Hemisphere above the Southern Hemisphere, the mesh arrays are alined so the grid line between the poles coincides with the 80° meridian. The present polar mapping program on the CDC 6600 requires 3.2 min of central processor unit (CPU) time (4.2 min, wall clock time) for each pole-to-pole hemispheric swath of input data. Nearly 100,000 sixty-bit words of high speed central memory are required, and the dedicated disk area for storage of the global map array is over 1.3 million 60-bit words. As an economic expedient, the 2048 x 2048 arrays are used in mapping both SR channels even though the spatial resolution of the visual channel data is substantially coarsened. Data are mapped as 8-bit quantities.

B. Mercator Mapping

The overlapped SR Mercator mapping for tropic and subtropic applications is similarly mapped at a common, coarser resolution. The orthogonal square mesh in this case is alined parallel to the equator with the far right column at the Greenwich meridian. The overall area covers the full earth circumference and extends from 40°N to 40°S.

The mesh size is 11.25 per degree of geocentric arc at the equator, equivalent to more than 5.3 n mi per mesh in the tropics. With the Mercator map, spatial resolution improves at the higher latitude extremities. Data are mapped as 6-bit quantities.

C. Limited Map Sectors with Augmented Resolution

Economics achieved through the coarsening of the mesh in the mapping described above render the data base useful primarily for mesoscale or

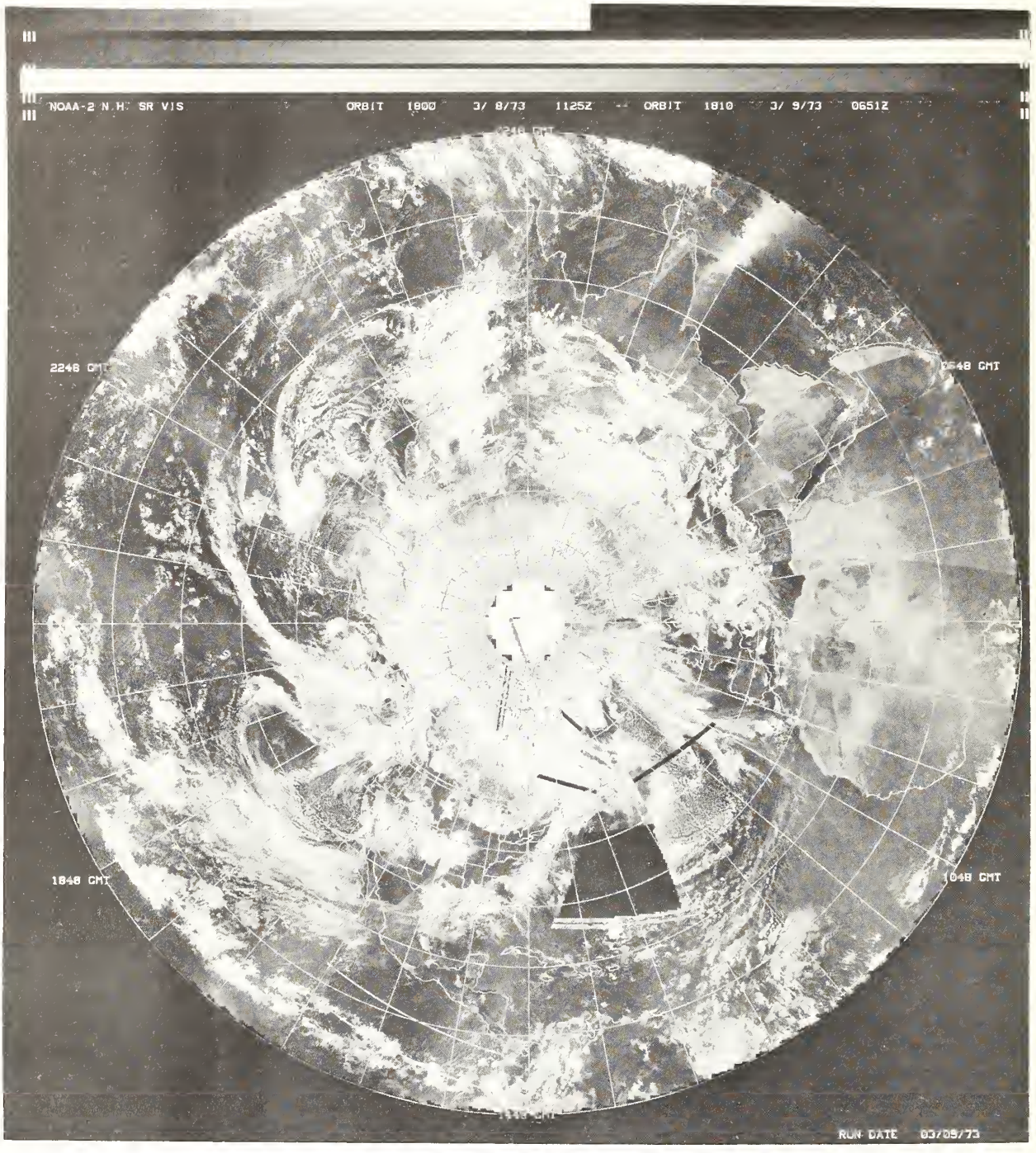

Figure 2a.--*SR visible data, Northern Hemisphere—typical example of mapped visible data in a 2048 x 2048, 8-bit array. Data void in Western Northern Atlantic is caused by physical limitations of the satellite orbit and ground station configuration. Other data voids are seen as black, white, or black and white areas, caused by tape parity errors, noise, and data breaks. Graininess in polar latitudes and marked discrimination between adjacent passes are caused by deficiencies in method used to compensate for angle effects.*

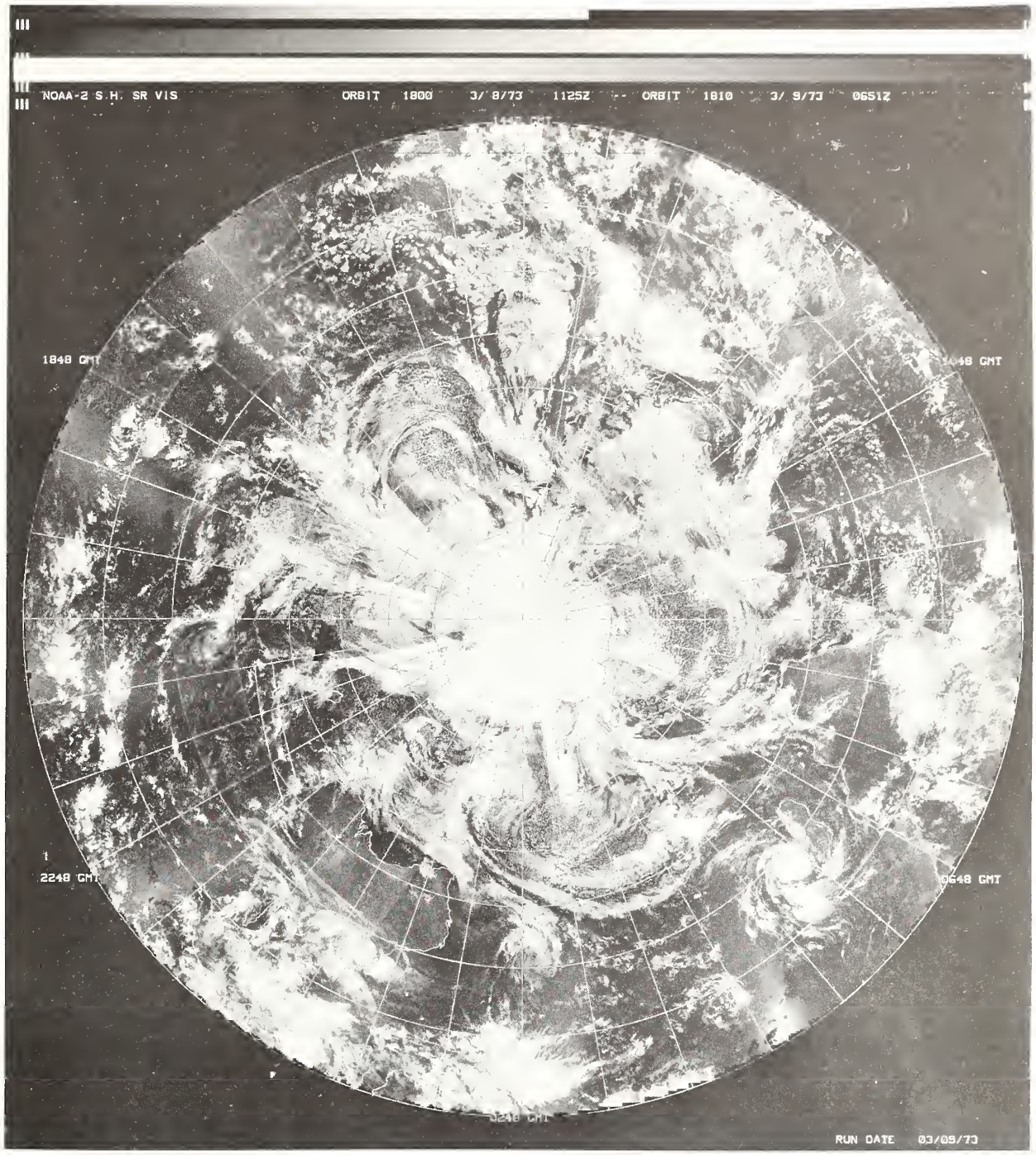

Figure 2b.--*SR visible data, Southern Hemisphere—typical example of mapped visible data.*

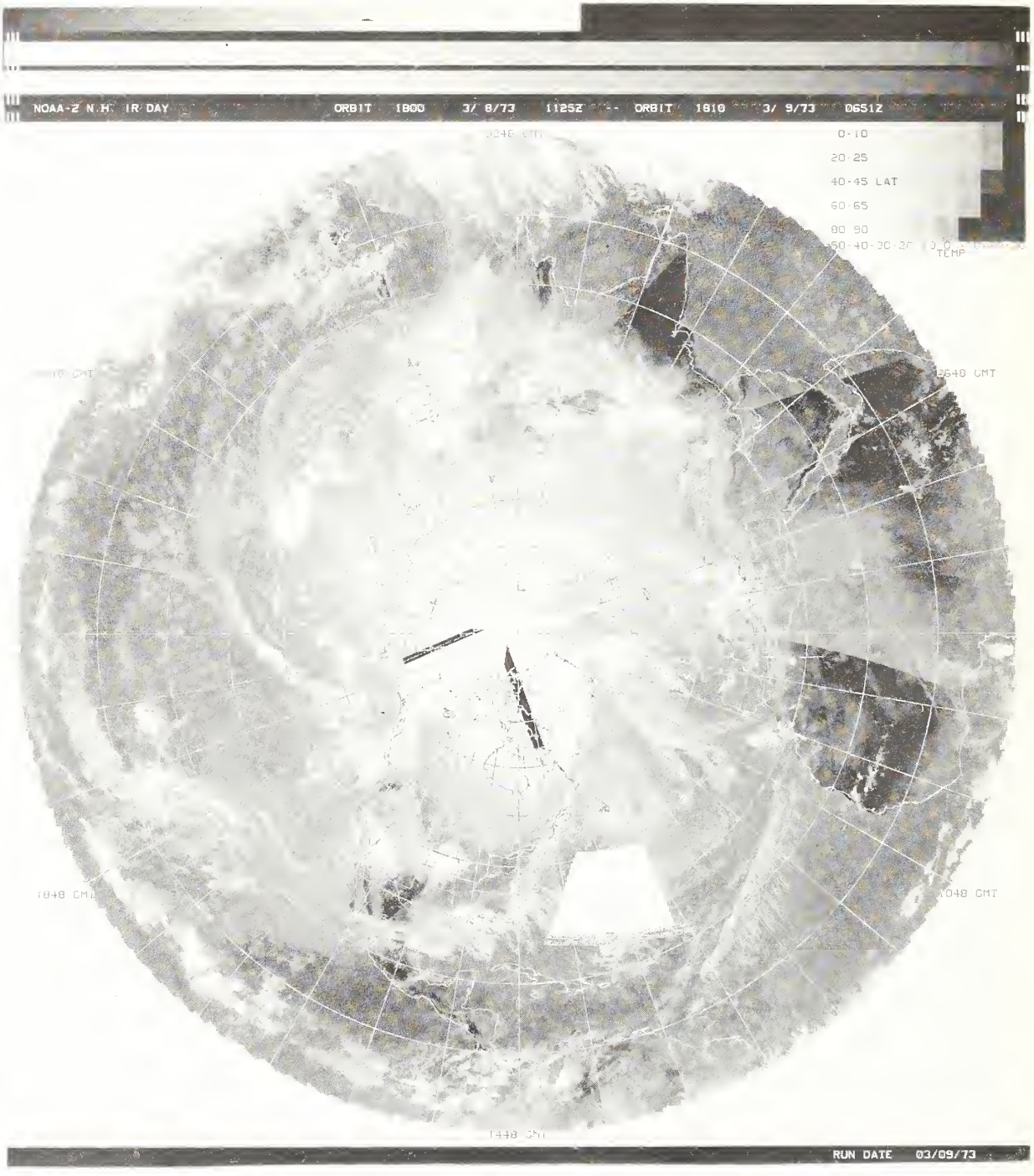

Figure 2c.--*SRIR daytime data, Northern Hemisphere. Typical processing void in the western North Atlantic is due to readout restraints. Black areas over Arctic are caused by data breaks; discontinuities are caused by time differences between adjacent passes.*

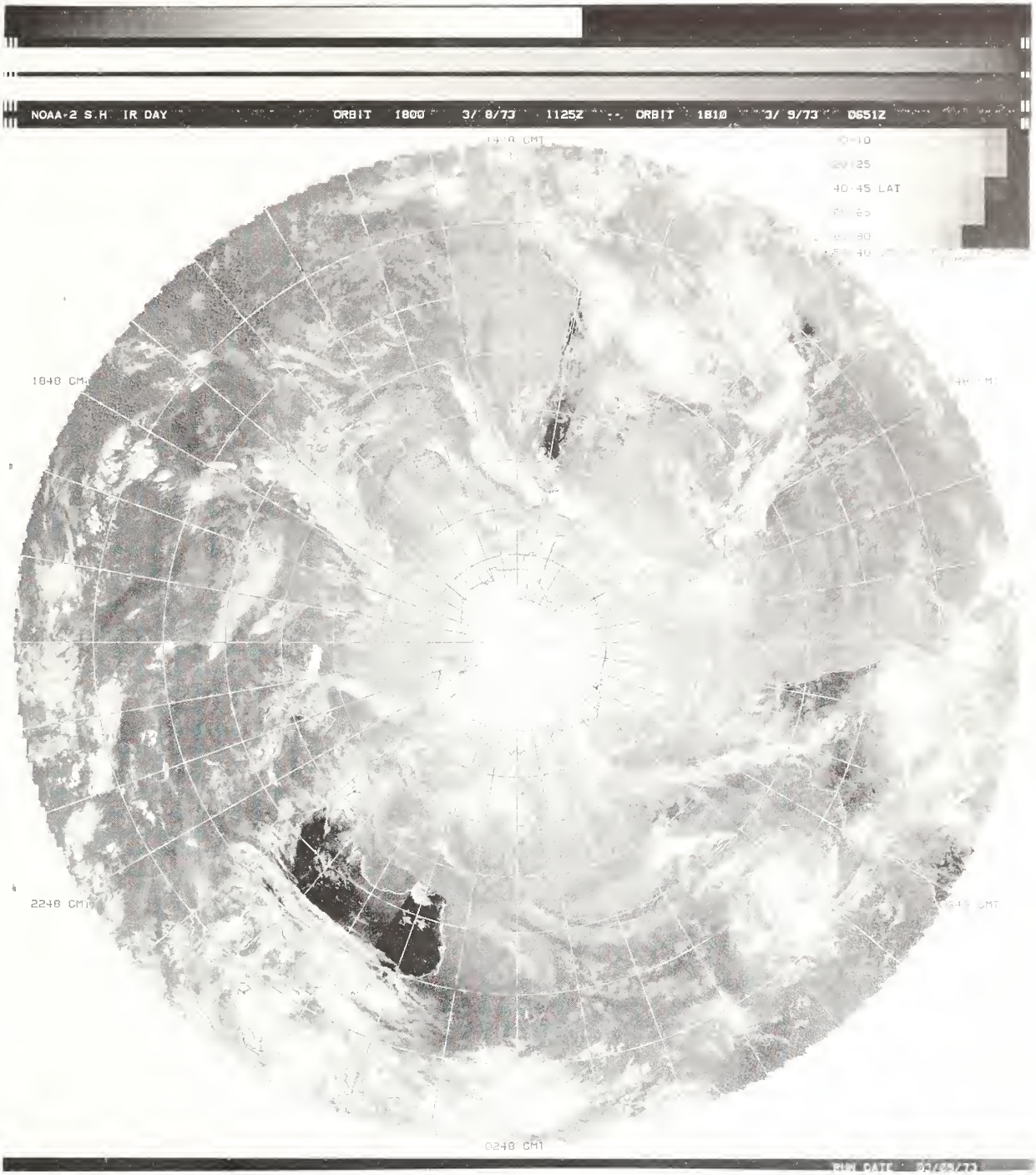

Figure 2d.--*SRIR daytime data, Southern Hemisphere.*

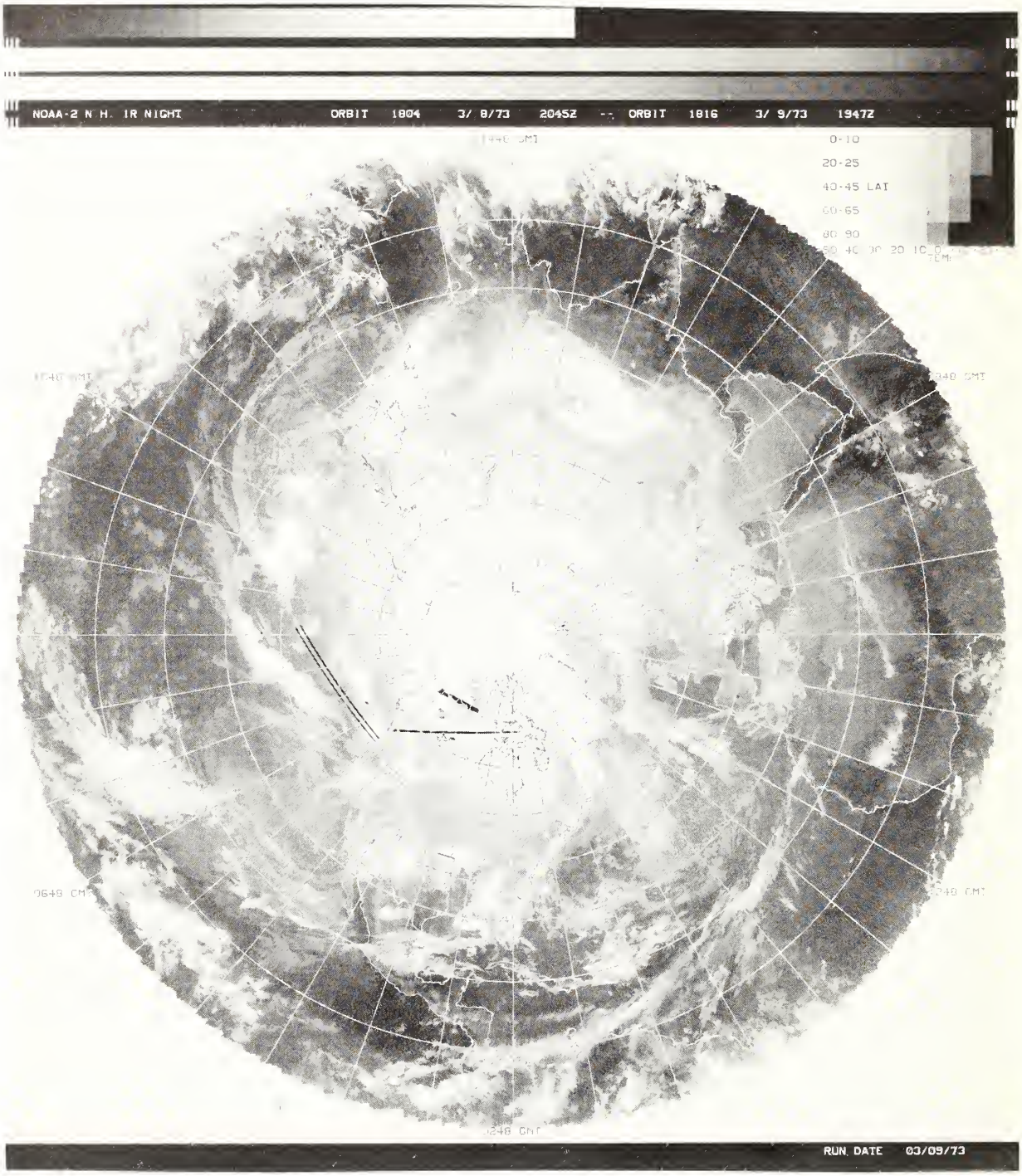

Figure 2e.--*SRIR nighttime data, Northern Hemisphere.*

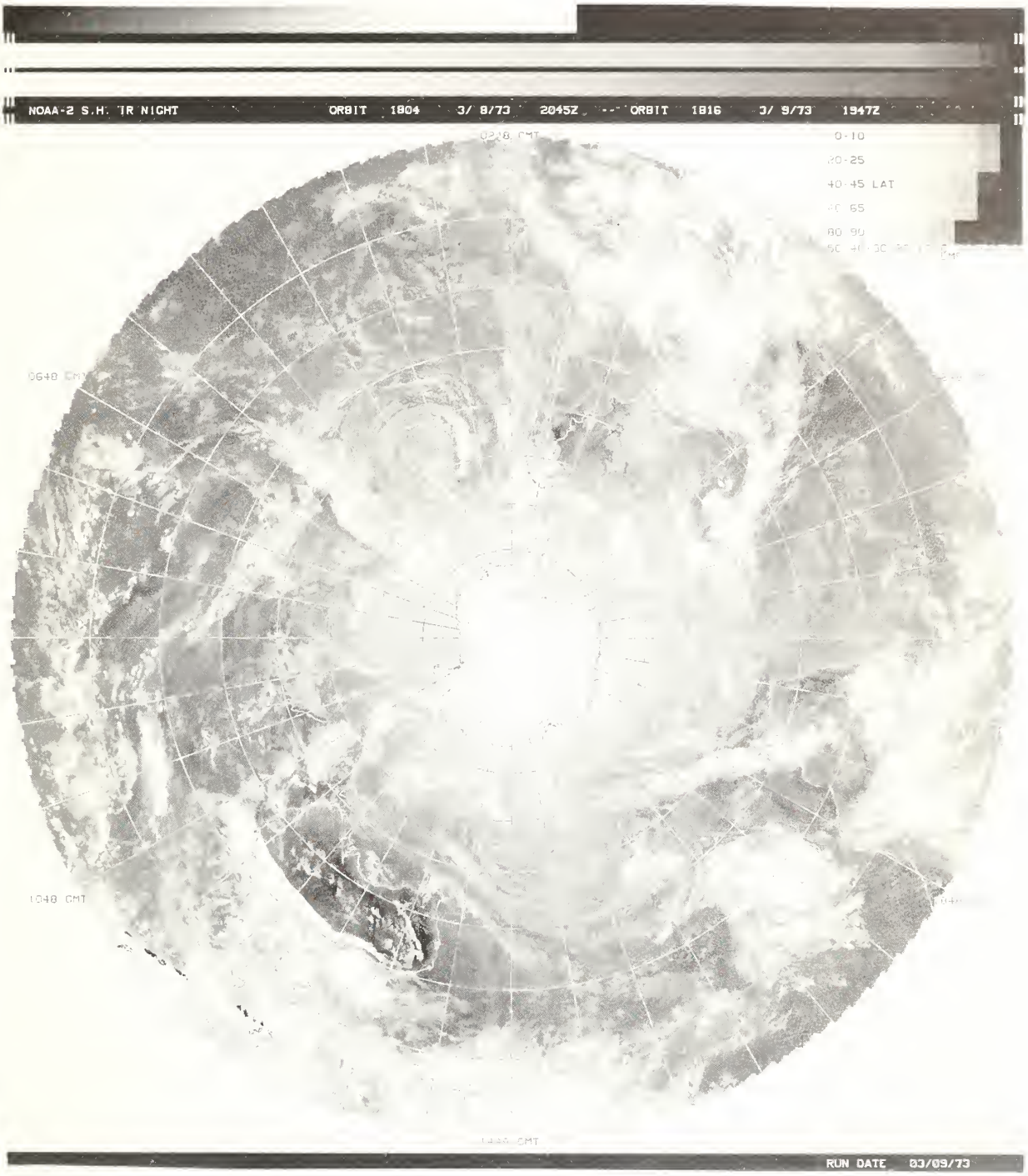

Figure 2f.--*SRIR nighttime data, Southern Hemisphere.*

macroscale applications. Therefore, certain sectors are mapped at higher resolution for specialized requirements using certain "universal" features of the basic mapper software. Such sectors can be produced with considerable flexibility. With mesh size set at 64 per NWP mesh (less than 4 n mi resolution at the poles), array size set at 896 x 512 elements, and center latitude-longitude coordinates selected, IR data are at present being mapped at optimum resolution for the sector shown in figure 3. Attributes of the display are described in the following section. Other finer mesh limited sectors can be produced. One small area has been mapped using 128 mesh points for each NWP mesh in conjunction with experimental midwest tornado applications. Another higher resolution, 20° x 20° Mercator sector with selectable center point location is available for hurricane analysis applications.

D. Individual Sectors Mapped by Orbital Pass

Apart from the polar and Mercator mapped image mosaics produced by the methods described above, there has been strong pressure to obtain mapped imagery with minimum delay. Accordingly, polar sectors are now being mapped on a pass-by-pass basis.

The principal customer is the recipient of image products sent via facsimile, so alinement of the image sector must be arranged to use the recorder display area most efficiently. Accordingly, the map mesh is rotated so the node longitude of the input data approximates the center axis of the map rectangle (as shown in fig. 4). With calibrated sample response truncated to displayable response range, this auxiliary mapping program needs far less frequent input/output service, so the computing time for the sector is reduced to 2.5 min per pass CPU time (4 min wall clock time). Sectors may be produced either from stored or directly transmitted SR data (DRIR).

E. Earth Locator Grids in the Perspective of Unmapped SR Imagery

Since image data mapping places greater dependence on computer resources, unmapped imagery will continue to fill a need. Despite the awkwardness caused by variable perspective, gridded strips of vidicon pictures with all the basic spatial resolution have been one of the most reliable and most promptly available products of past ITOS satellites. Although pass-by-pass mapped SR products are expected to fill much of this requirement, there will likely be continued interest in imagery displayed in the perspective and retaining all the spatial resolution of the original signal. In line with this need, strips of unmapped SR imagery are also produced on a pass-by-pass basis.

By a rearrangement of the equations for bench point earth locations, one obtains image line spot coordinates corresponding to integer latitude-longitude points. By selecting an adequate population of such computed points and interpolating filler points, latitude-longitude lines and geographic outlines can be produced and melded with the unmapped images. Figures 5a and 5b are samples of the same data. Scan lines and individual samples are replicated to yield an aspect ratio near 1-to-1 and to compensate for the foreshortening effect due to scanning geometry. Such stretched orbital strips have replaced the equivalent gridded vidicon image strips.

Figure 3.--*SRIR augmented chip showing Arctic areas of North America and Greenland.*

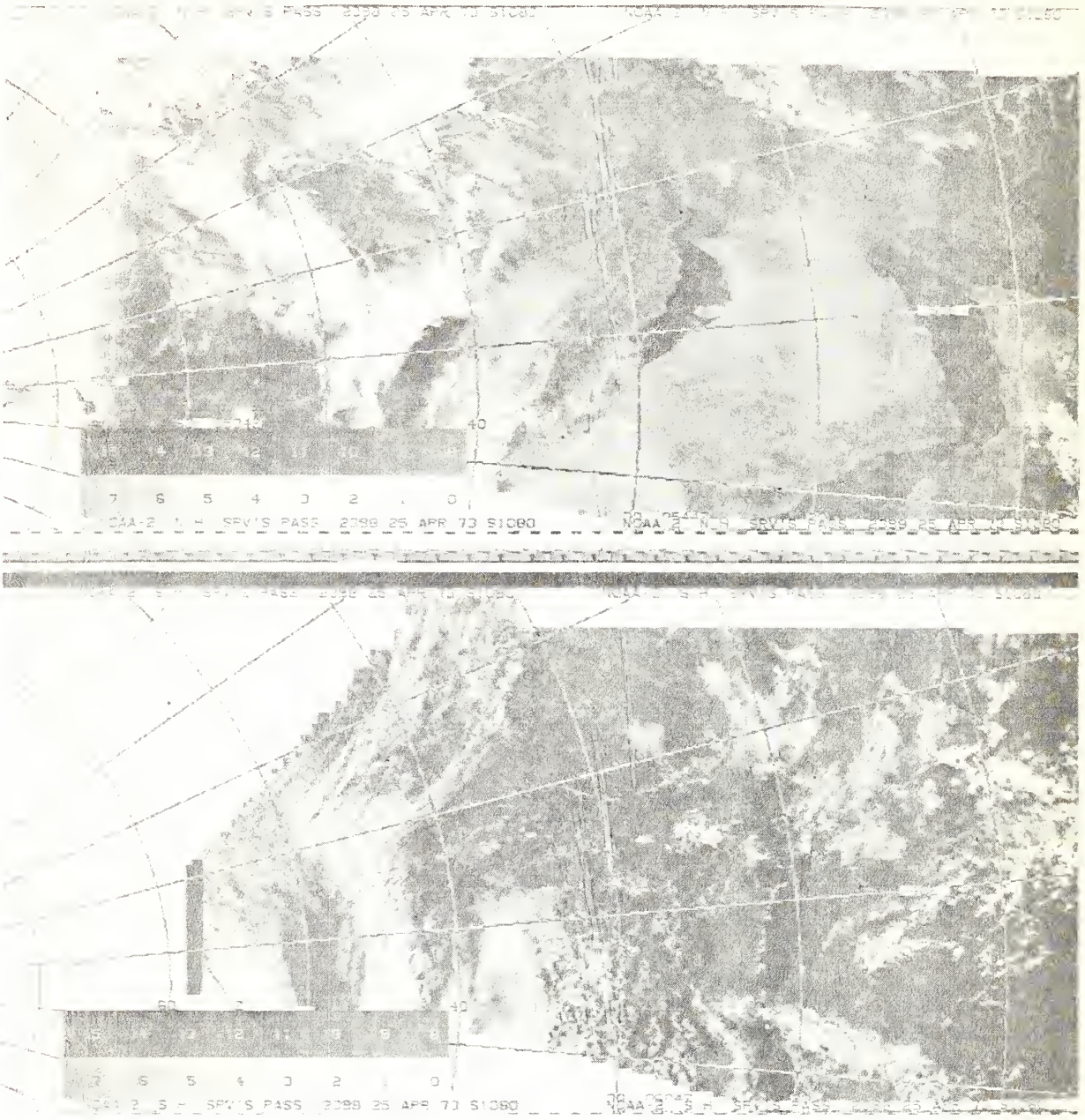

Figure 4.--*SR visible pass-by-pass facsimile. These are photographic copies of material received from a standard Alden facsimile machine of pass 2398, April 25, 1973.*

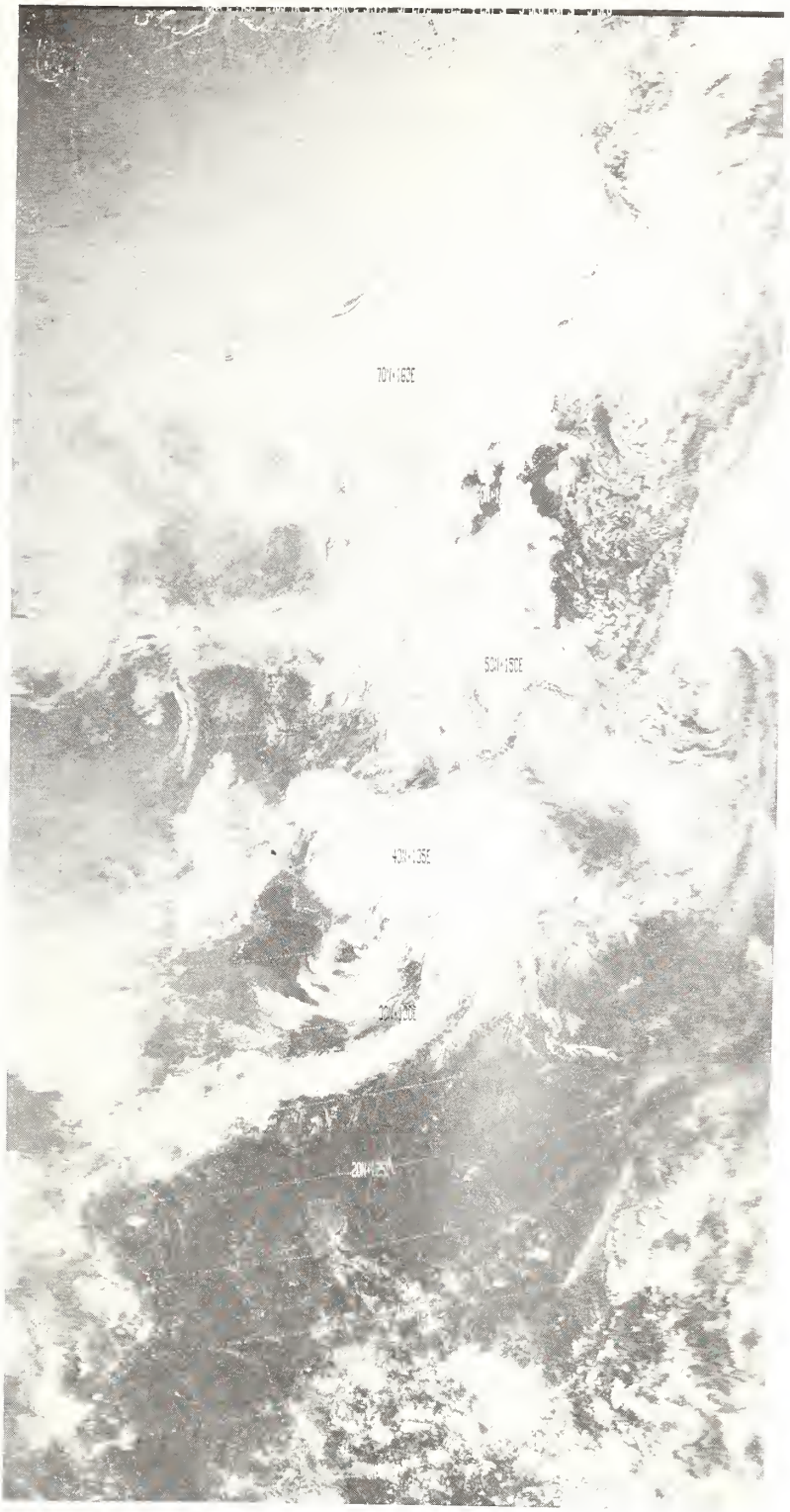

Figure 5a.--*SR visible, stretched and gridded pass-by-pass data. Figures 5a and 5b are the effectively lighted area covered by the visible channel of the SR during one pass. Data for 5a and 5b are continuous.*

Figure 5b.--*Continuation of 5a.*

F. Earth Location Precision

In general, the earth location of image data through the processes described above can be regarded as a direct function of the accuracy of the various input parameters. That is to say, the precision with which calculations are made (generally 60-bit floating point precision) and the realism involved in any parameterization (for example, use of an oblate earth model in transforming spacecraft related position vectors to geocentric coordinates), causes position accuracy to depend primarily on the precision of orbital position determination and the accuracy of other input items. A discussion of the precision with which the numbered items in the preceding section are obtained provides a semiquantitative basis for estimating the overall earth location accuracy of the SR data.

The specification of satellite position as a function of time involves the use of volumes of tracking data as input to an orbital model. The mean orbital elements determined from this model serve as input to a less sophisticated prediction model that specifies the three dimensional spacecraft position vector for some future time--typically for some 2 to 3 weeks beyond the time span of the tracking data from which the original elements were determined. Although separate position determination comparisons have not been made in conjunction with this image earth location procedure, the intercomparison of earth position predictions, using preceding and current orbital element groups, yields answers that practically coincide. Specifically, the equator crossing time for a particular orbital pass, as predicted by two sets of orbital elements one week apart, will typically agree to within less than 1 second (with a 115-min orbital period, 1 second of spacecraft travel represents about 3.1 mi in sub-point position). Satellite altitude differences for such pairs usually are 1 mi or less and rarely exceed 2 mi. Therefore, good stability is indicated in predictive spacecraft position. If the predictive differences are interpreted as indicators of absolute position uncertainty, then overall horizontal accuracy is about $\pm$ 2 n mi. Horizontal positioning errors arising from errors in satellite altitude prediction are of secondary importance only (see attitude discussion below).

In the case of the scan mechanism, there is again no ready means for validation of sweep orientation with respect to the spacecraft. There is only obvious pictorial evidence that the mount has not changed to a noticeable degree.

The spin phase angle between the porch injection point and the spacecraft base plate may be discussed in conjunction with the angular increment considerations. Ideally, if the baseplate orientation could be determined by some independent means, then the porch would become an absolute reference. Then some specified sample farther along the spin cycle could be specified as the first earth viewing sample, and precise knowledge of the angular increment per sample would permit placement of all subsequent samples until the final earth viewing response was properly positioned.

In practice, the porch serves only as a spin phase cycle reference in attitude determination (see below), and the stability of its phase position, rather than its absolute phase angle position, remains the critical factor.

As mentioned earlier, the spin phase angular increment determined for each sample depends upon scan shaft spin rate and sampling rate. The 48-rpm scan rate is verifiable by multiplying the sampling rate by the number of samples detected between occurrence points of the porch and dividing the product into 60; this technique gives the correct scan shaft spin rate in RPM.

The sampling rate is controlled by a voltage controlled oscillator (VCO) that is normally very stable. Limited checks indicate agreement to within one sample between populations of samples in adjacent spin cycles (porch-to-porch). In abnormal drift situations, VCO malfunction is evident through software-assisted diagnostic procedures. SR data recorded aboard the spacecraft suffer nonlinearization because of recorder speed variations (flutter and wow). A separate, constant tone recording on an accompanying channel provides the means for relinearizing the sampling rate. The nominal compensation (accomplished through flutter and wow induced variations in the sample rate controlling VCO) is to within 0.25%. Thus, the local distribution of approximately 1,200 samples per earth traverse may be nonlinear by as much as 4 samples, despite the seeming stability in overall sample count per spin cycle.

Attitude was discussed in some detail. Here mention is made of the obvious dependence of the porch-to-horizon roll/yaw measurements upon flutter and wow (F/W) and sample rate control. Limited tests using specified sampling rate, scanner spin rate, and F/W compensation have produced base-plate-to-porch angle estimates that agree with prelaunch alinement specifications. In practice, roll/yaw measurements are adjusted by means of an iterative procedure so there is no residual bias in roll/yaw through an orbital pass. The results are thus rendered immune to the specific porch phase angle so long as the porch position remains stable. In discussion of spin axis orientation, roll component error is expressed as a radial distance error with respect to the subsatellite point, whereas the equivalent yaw error (a quarter of the distance around the orbit) appears as a tangential (azimuthal) error in image positioning. The two effects have been discussed together although, in magnitude, the radial error component tends to predominate (Bristor et al. 1961). The great advantage in this attitude determination method is the availability of such measurements throughout the entire orbit. By using local averaging (every 25 spins) and a least-squares fit for the entire orbital cycle, the stability of the attitude estimate is good as indicated by the close agreement between estimates from contiguous orbital passes. This suggests that the right ascension and declination of the spin axis are specified to an accuracy of approximately 0.1°. Horizon sensing supplies error signals to a continuous pitch control mechanism; these error signals are available for analysis on the ground. Unfortunately, samples of these signals have been noisy, so no definitive analysis has yet been made.

Table 1 provides insight as to image earth location error introduced by attitude error and by orbital altitude error. Specifically, differences in geocentric distances from the subsatellite point (errors) are presented for 0.1° roll/yaw changes for various spin phase nadir angles at the spacecraft. And in each case, the equivalent altitude difference (error) has been computed. For example, with the scan mirror pointing 10° from the subsatellite point (viewing a point less than 150 n mi from the orbital track), an error of 0.1° in roll/yaw introduces a location error of about 1 n mi. With perfect atti-

Table 1.--*Earth location error resulting from attitude and altitude errors*

Spin phase nadir angle at spacecraft (degrees)	Equivalent geocentric arc distance from subsatellite point (degrees)	Geocentric error increment for 0.1° roll/yaw error (n mi)	Equivalent spacecraft altitude* error (n mi)
10	2.2	1.2	41.4
20	4.6	1.6	20.1
30	7.5	2.0	12.7
40	11.5	3.0	8.7
50	18.9	7.2	6.2
55	32.1	13.8	5.1

*Nominal orbit altitude 750 n mi

tude, the equivalent location error arising from erroneous spacecraft altitude would involve an altitude error of 41 n mi. Image elements sensed far from the subsatellite point (over 1000 n mi at 50° nadir angle) would be located in error by approximately 10 n mi with an attitude error of 0.10. An error in spacecraft altitude would be about 5 n mi for the same effect.

Finally, the precision with which time is specified depends upon the initializing accuracy and the precision of the basic clock oscillator. Procedure for spacecraft clock reset provides for strip chart recording of command pulse together with absolute time code. By use of this chart, the moment at which the spacecraft clock is reset can be estimated to within about 0.1 second. Since the spacecraft clock counts in quarter-second increments, the absolute time reference can be established well within the granularity of count, resulting in earth location precision of about 0.4 n mi. Long term accuracy of the spacecraft clock can be verified by comparison with precision ground measurement over an extended time base.

Overall error normally is indicated by combining the separate components. The incomplete and only semiquantitative discussion above might best be summarized in terms of an educated guess as to the practical precision in earth location of SR imagery. Additional diagnostic checks are to be carried out, and a longer period of stable operations is needed before precise figures can be obtained.

Based upon present evidence, however, it seems that most SR imagery is being located with an accuracy of about 10 n mi or better near and along the orbital track. In the foreshortened scan regions, this range of error may double. Since coastline and other land form features are melded with earth located images, one may often check the location precision.

Equivalent earth location errors for vidicon imagery from ESSA spacecraft have been quoted as 30 to 60 n mi. There are reasons to believe that SR location error figures are better because:

a. Absolute time is obtainable for SR data frames, whereas ESSA vidicon picture times were deduced from an accumulation of spin rotations of a spacecraft undergoing cyclic spinup and damping accelerations,

b. horizon scan sensors for attitude determination on ESSA spacecraft provided less frequent and lower quality observations for limited sectors of each orbital pass, and

c. scanner geometry is less complex than the equivalent two-dimensional distortion pattern needed for the conversion of vidicon image X,Y locations into orthogonal angle components in object space. Since the sources of error in locating SR data all seem to range from 1 to 3 samples in uncertainty, the implication is that no major improvement in location precision will be reached without a complete systems approach to the problem.

6. PRODUCTS

A. Noise

Before discussing products, brief mention should be made of noise present in the SR data recorded on the spacecraft. Since scan mirror rotation and the tape recorder drive motor are controlled by a common power source oscillator, the noise related to the recorder tends to be periodic. Therefore, although within nominal specifications, the noise tends to create systematic streaking in display products (fig. 12) and to produce systematic contamination in the generation of more quantitative applications (Bristor 1970). Figures 6a and 6b are histogram portrayals of the noise pattern from one tape recorder on NOAA-2. The distribution of absolute responses and the distribution of differences of adjacent sample pairs is shown for a supposedly inert recording of nighttime data from the visual channel scan sensor. A more exhaustive analysis of tape recorder noise, based on ITOS-1 data and its distribution in the spatial frequency domain, is provided by Leese et al. (1971a). A substantial noise reduction has been effected without major spacecraft modification by modifying ground station hardware. The ground station modification takes advantage of the fact that the F/W channel recording contains the same noise pattern as the video data channel. In essence, the F/W channel noise pattern is used to correct the accompanying SR sensor response. With suitable delay adjustment, this Z-axis correction removes much of the systematic noise.

B. Visual Products

Image products from the TOS spacecraft have been described in various papers (e.g., Leese et al. 1970). A catalog listing and describing all ITOS products of the NESS Data Processing and Analysis Division is to be issued shortly.

In the case of visual products, a photofacsimile recorder provides the source for imagery distributed for local real-time use and for nonreal-time mail

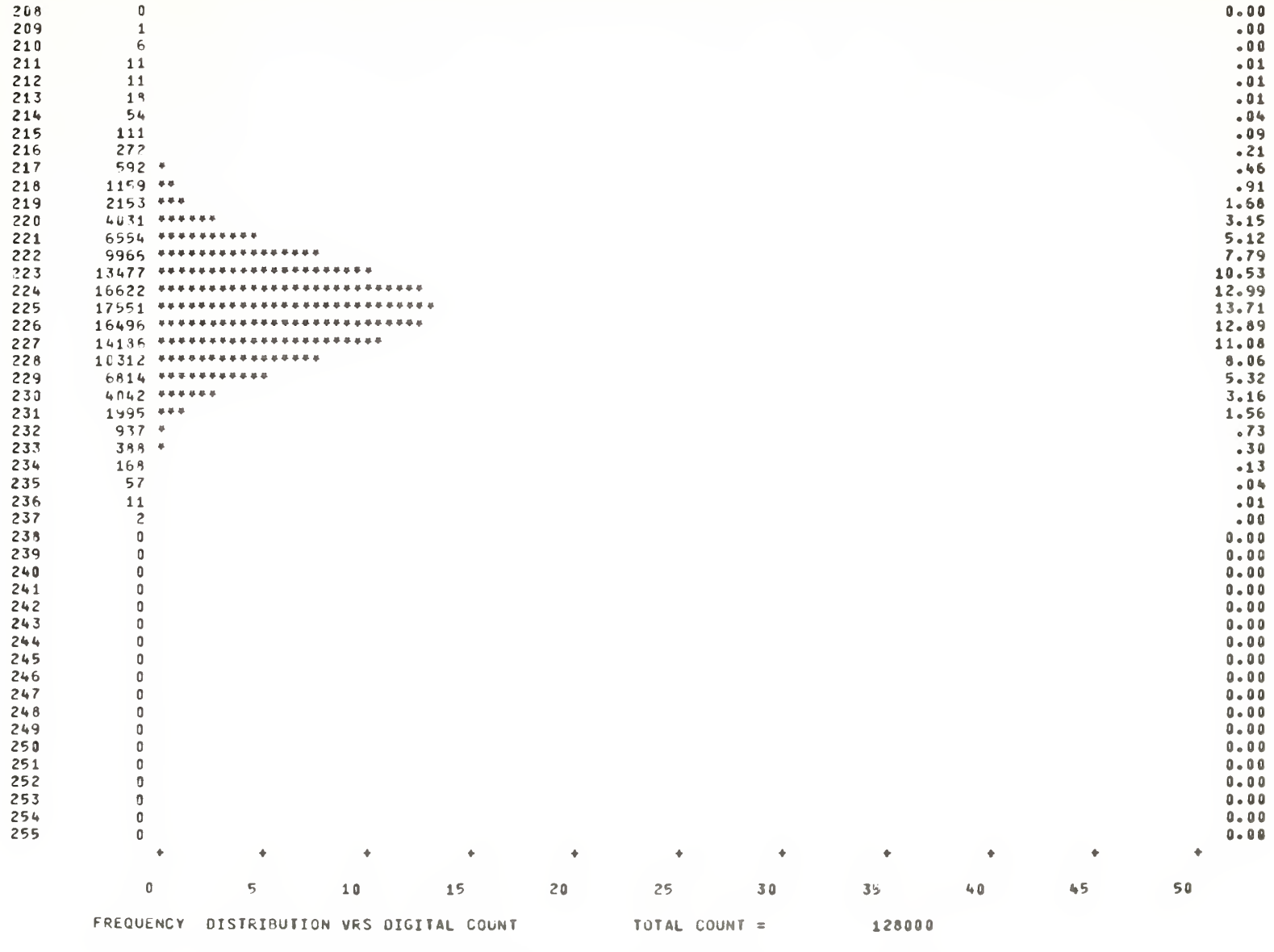

Figure 6a.--*Noise outline, NOAA 2 tape recorder (absolute response).*

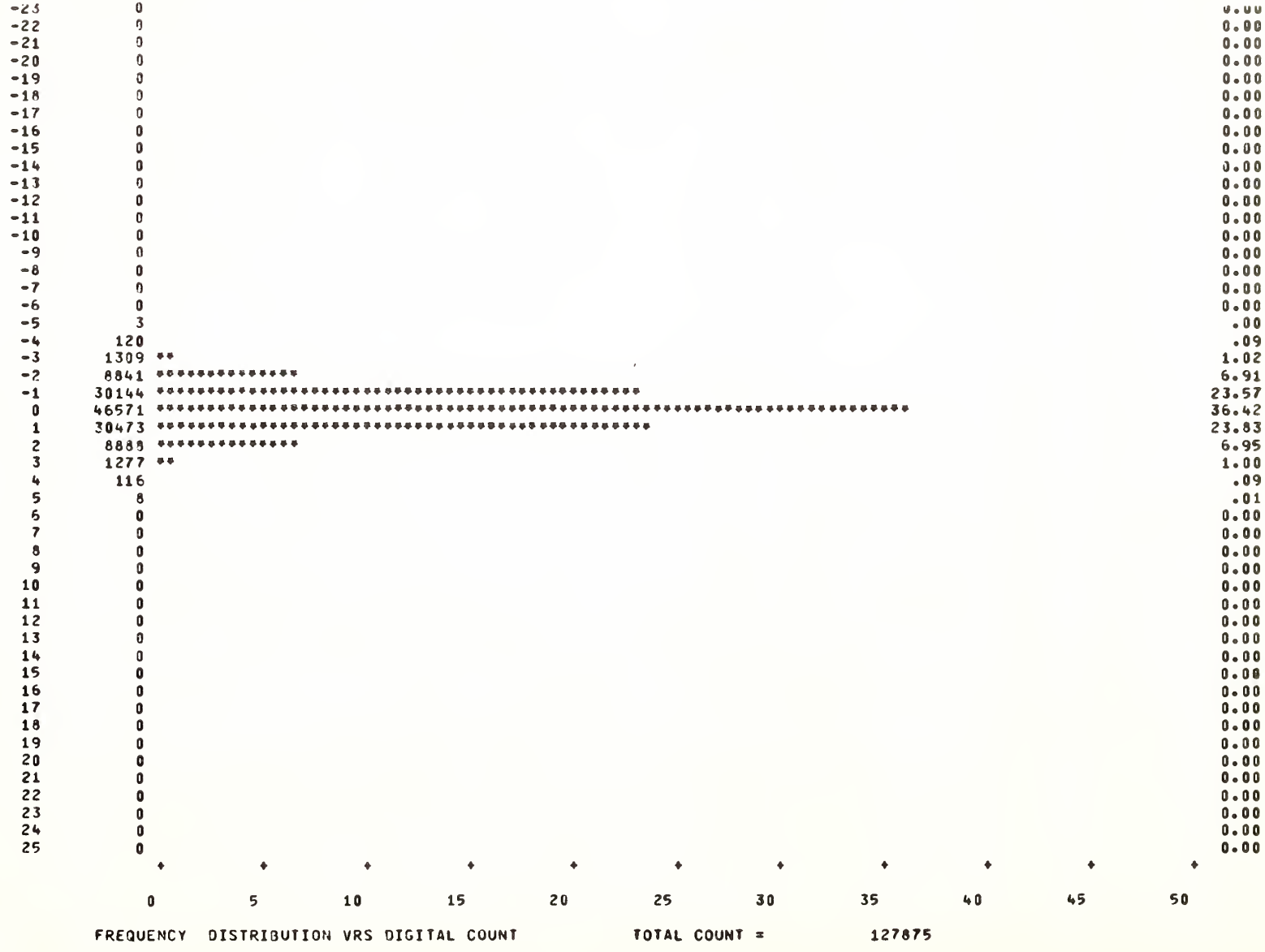

Figure 6b.--*Noise pattern, NOAA 2 tape recorder (absolute response).*

distribution. Both polar and Mercator mapped products are displayed on this device. Figures 7 and 8 are samples of the Mercator presentation for IR and visual data respectively. Display capability from digital source material is available in 2500- and 5000-line modes using a nominal 10-in. negative size. Six-bit (64 gray levels) display samples serve as input.

Other visual products are distributed to standard 18-in. weather facsimile recorders. Again, a digital image tape is the source, and display scan sample populations are converted to analog facsimile scan signals through an encoder device. Some 50 image product transmissions are scheduled daily. Sample populations are limited to 1710 per scan line and normally are displayed at 96 samples per inch (line-to-line and sample-to-sample). Only 16 input gray levels are provided by the 4-bit sample size. Weather facsimile samples are shown in figures 4 and 9.

Display products are also formatted for receipt by APT receivers, again using the facsimile encoder in an alternate mode. Again the samples are 4-bit bytes, but the display is restricted to an 800 x 800 array. The standard APT recorder provides 8-in. square hard copy. Quality is somewhere between that provided by photo and facsimile recorders (fig. 10). These products are relayed to ground network APT recorders and to radio receiver APT stations via geostationary spacecraft (ATS-1 and ATS-3) relay.

C. Gray Scale Presentation

The choices of gray scales used for image display of the ITOS data are aimed at depicting the maximum information possible, given the limitations of the display equipment. Both the visible and thermal radiometer channels are digitized over a range of 256 levels while the display equipment is limited to 64 levels for photographic display and 16 levels for facsimile; hence, compression algorithms are required for the production of image outputs. First, both the visible and IR are converted to coded, 8-bit values for archival purposes (tables 2 and 3). Coded values are then relabeled as display system output levels; the output levels constitute the gray scale. A joint user group, composed of representatives of the NWS, NESS, U.S. Navy, U.S. Air Force, and research meteorologists, selects the particular gray scale used for any given display product.

The outlined method of transforming raw sensor data to coded values to output device gray scale levels provides for a maximum of flexibility. The method is insensitive to differences in source data, and gray scales can easily be modified to meet new requirements for output displays. Proven usage should eventually lead to a stabilized set of scales for operational products.

D. Derived Products

All the display products shown previously are obtained as simple byproducts of the image mapping operation. The SRIR data are also used for generating quantitative products. While such processing is designed for digital applications, these derived products may also be displayed in pictorial formats. One current effort involves the generation of mapped cloud distribution in three dimensions using the infrared mapped data as a source (DeCotiis and Conlan 1971).

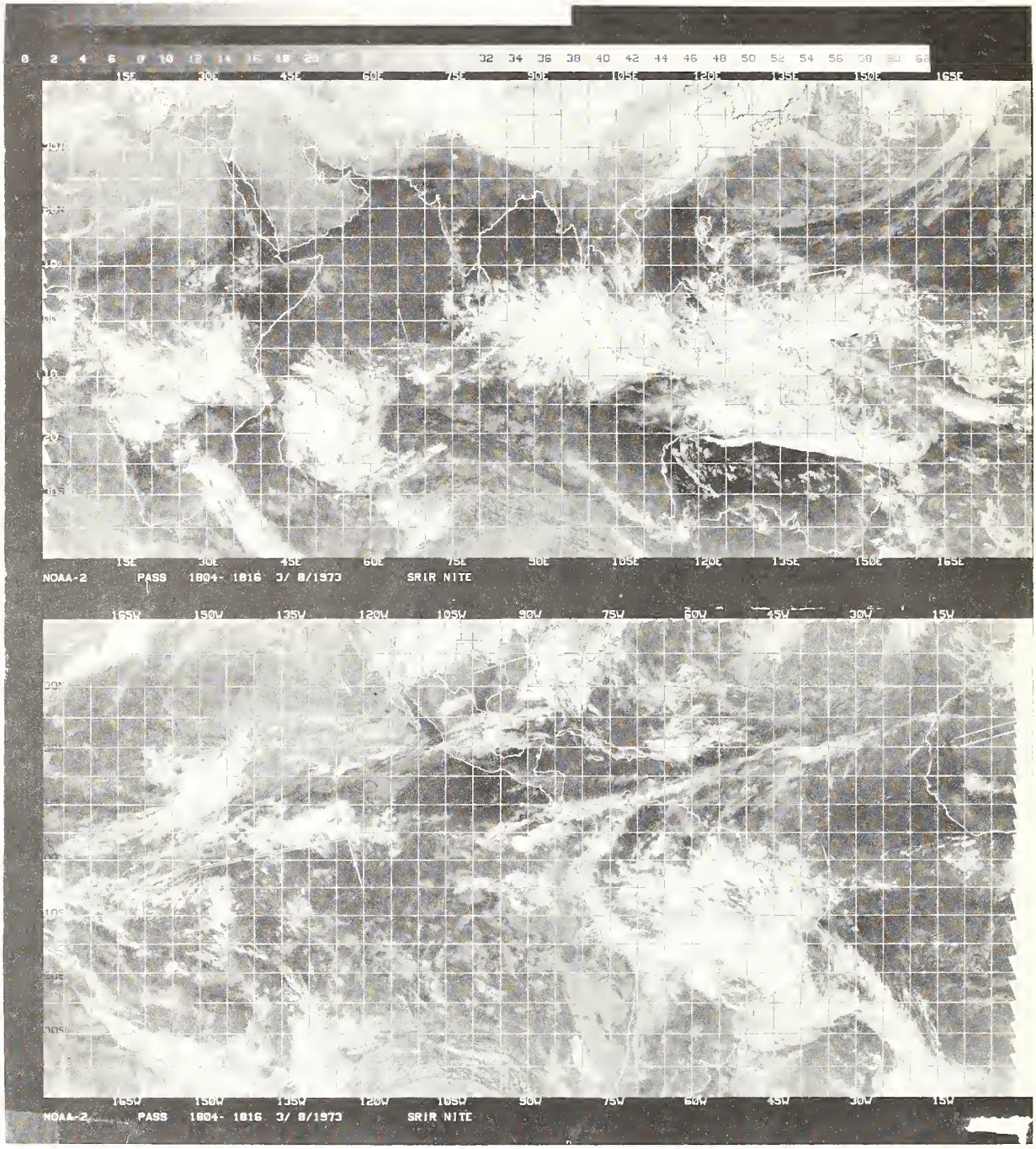

Figure 7.--*SRIR nighttime data (Mercator projection). Data from orbits 1804-1816, March 8, 1973. Data voids show as white areas.*

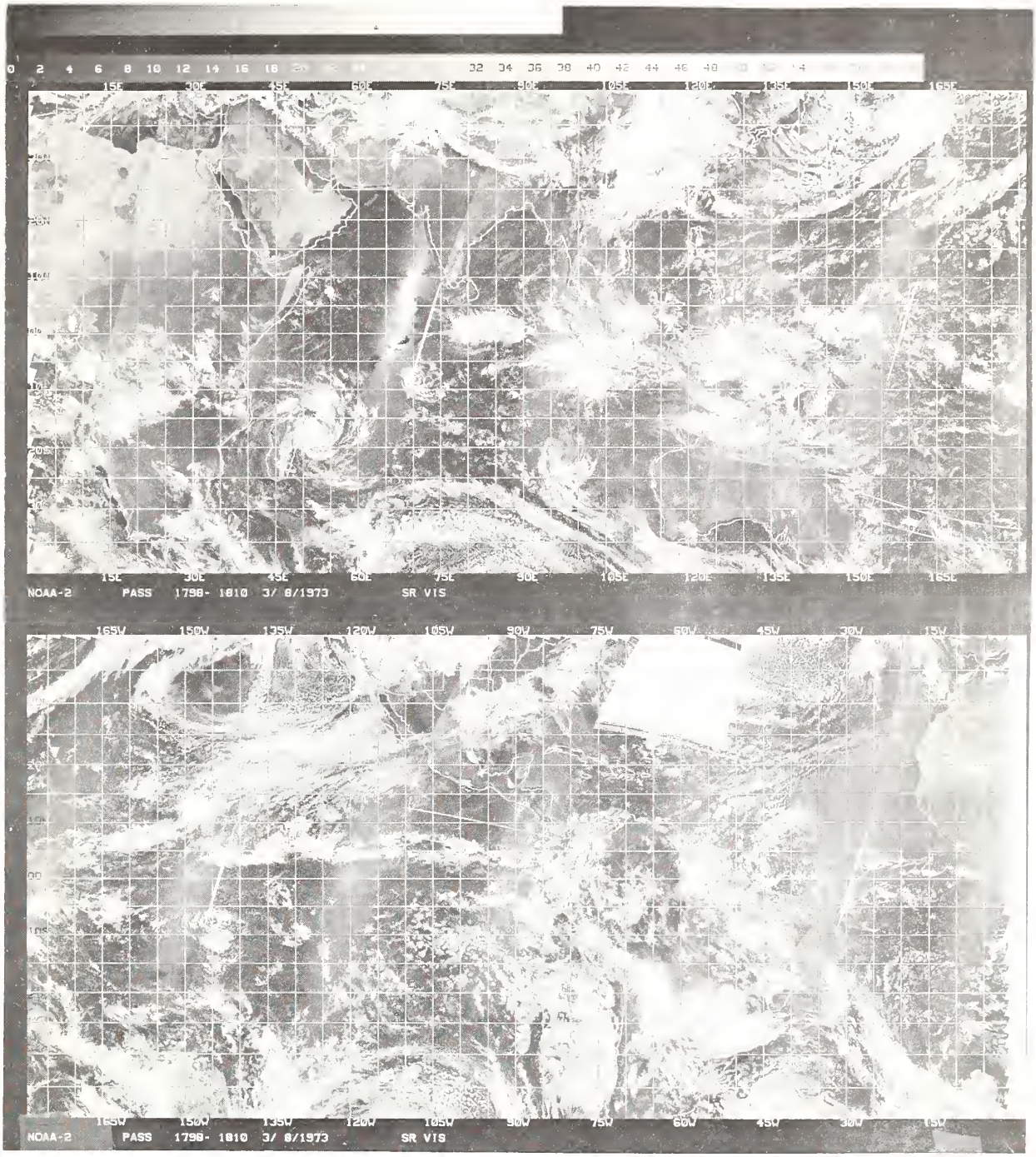

Figure 8.--*SR visible data, orbits 1798-1810, March 8, 1973. Mercator projection.*

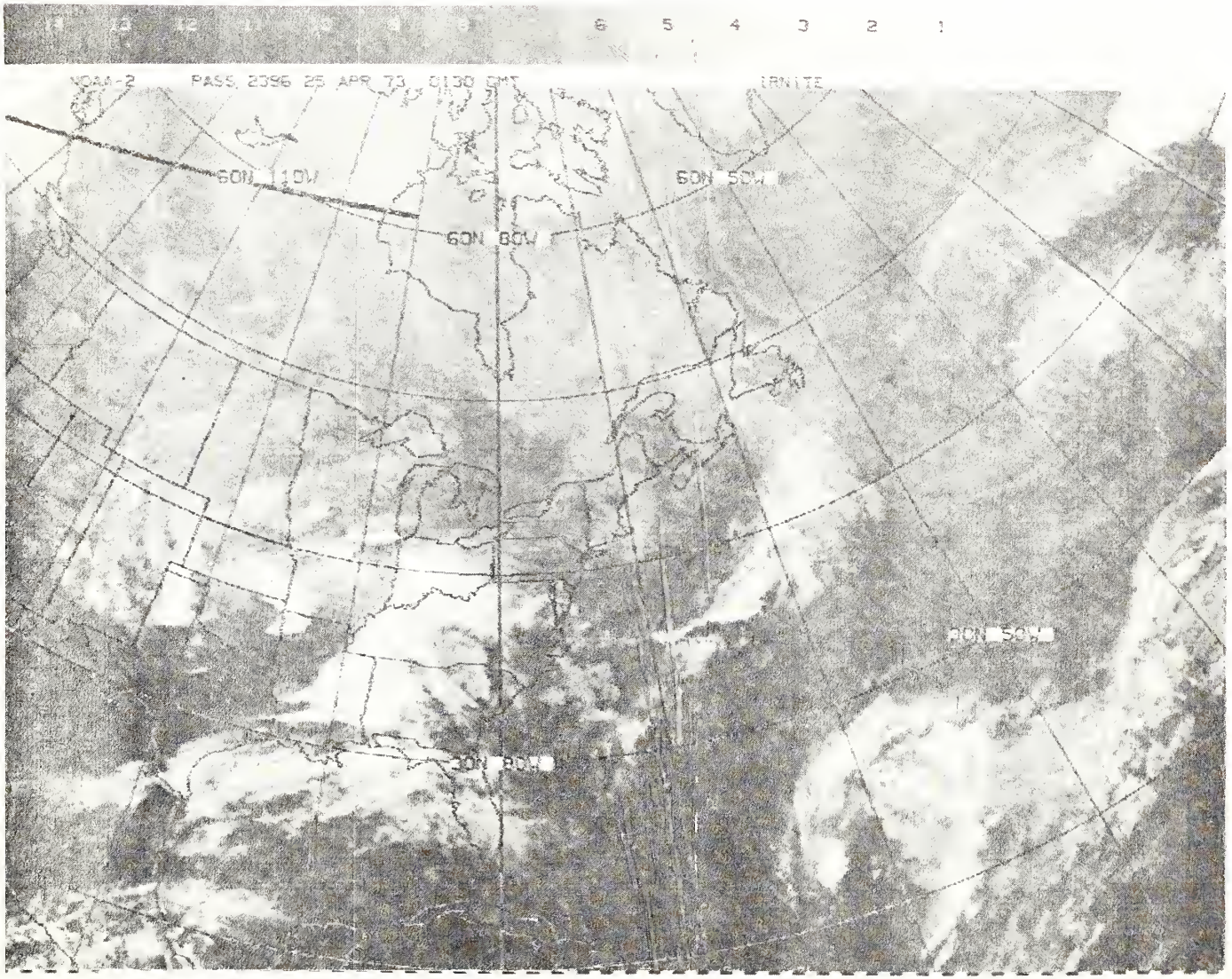

Figure 9.--*SRIR nighttime facsimile chip, April 25, 1973. Photographic copy of data as recorded on a standard Alden facsimile machine.*

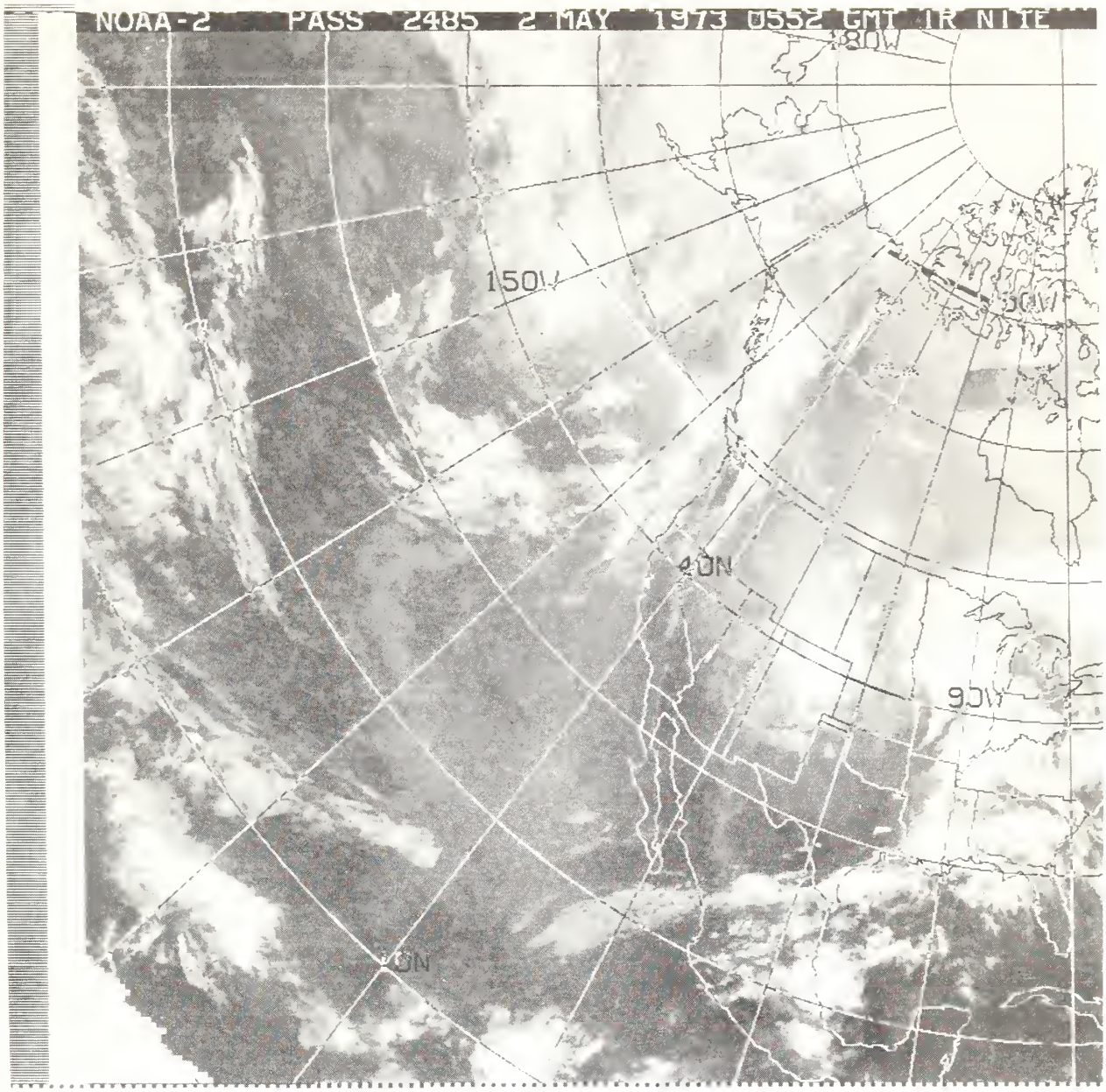

Figure 10.--*WEFAX picture received on APT from ATS WEFAX broadcast. Several charts in either Mercator or polar stereographic projection are transmitted during each broadcast. Data can be either SRIR or SR visible.*

Table 2.--*Conversion of foot lamberts to coded values--visible data*

Foot lamberts	Coded value
0 - 34	0
40 - 79	1
80 - 119	2
120 - 159	3
.	.
.	.
.	.
10,020 - 10,059	254
10,060 - 10,099	255

Table 3.--*Conversion of temperature to coded values--IR data*

Temperature °K	Coded value
164.0	0
165.0	1
.	.
.	.
.	.
242.0	78
242.5	79
243.0	80
243.5	81
.	.
.	.
.	.
310.0	255

Using temperature and height estimates obtained from objective weather analyses, the SR radiative temperature responses mapped within each NWP square are classified in terms of clear conditions, and low, middle, and high cloud responses. Apart from contoured visual display (fig. 11), such processing provides percentage estimates of cloud cover in digital tape format for each NWP square population. In addition to current operational use, extended records of such information can also be used in a variety of synoptic-climatological applications (Miller et al. 1971).

The generation of sea surface temperature is another important new application. The problem in this case involves the elimination of cloud contamination. Adjustments to the basic method (Smith et al. 1970) are described in conjunction with the above mentioned noise in the SR signal by Leese et al. (1971a and 1971b). The error in sea surface temperature production is a function of noise filtering (smoothing) and tests to exclude sectors with heavy cloud contamination. Using the current operational algorithm, overall sea surface temperature products are estimated to have an RMS error of 1 1/2° to 2°K. Such production can be used directly as input to NWP models and as surface reference in the utilization of indirect sounding radiance data.

The infrared SR data are also being utilized in sea and lake ice reconnaissance (McClain et al. 1969). Imagery with extreme enhancement in the critical ice water temperature zone is providing a tactical support tool (fig. 12). Digital output from such sectors, mapped at higher spatial resolutions, is providing a data base for more quantitative treatment.

A variety of developmental activities is proceeding, but without current operational production. The following are among those now under development:

a. Multi-day compositing of mapped SR image data is expected to have application in hydrology as indicated by earlier efforts using TOS vidicon data (McClain and Baker 1969). Current compositing experiments to save the warmest infrared response offer promise.

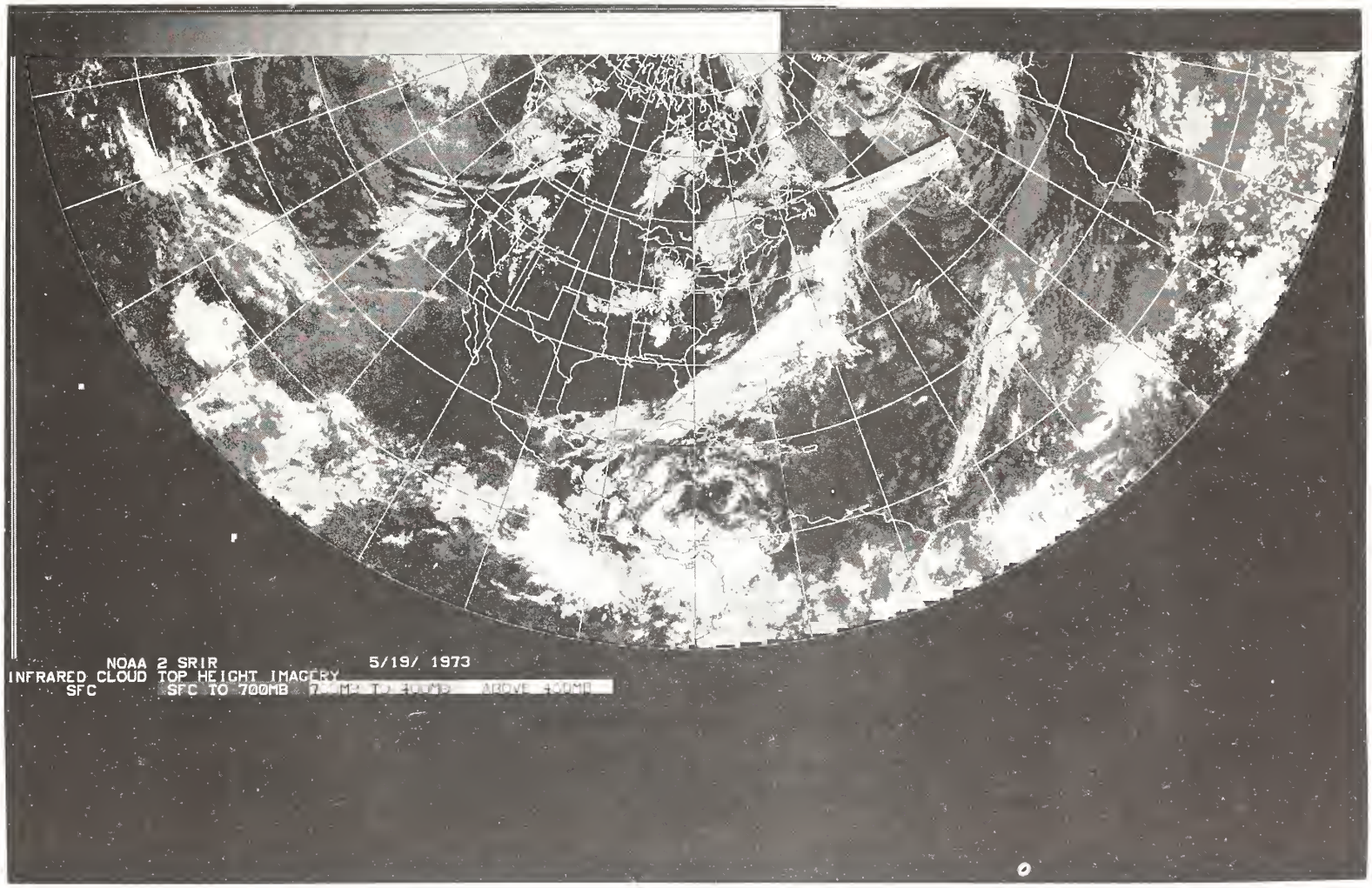

Figure 11.--*SRIR-derived daytime cloud-height data. Pressure-height information from NWS data.*

Figure 12.--*SRIR data formatted for ice identification analysis. Digital enhancement added in critical ice/water temperature range. Temperature above 32°F(0°C) shown in black. Data for January 14, 1971.*

b. Semiobjective estimates of mean moisture in the troposphere are currently being obtained from mapped data by skilled nephanalysts (Smigielski and Mace 1970). The additional cloud height discrimination provided by the infrared SR data should substantially improve skill in this area. As concurrent visual and infrared SR data become available in mapped form, an earlier attempt at computer determination of moisture content will be reviewed.

c. A great potential also appears to exist for the quantitative and objective description of tropical cloud systems. Over the years, cloud imagery has proven to be of substantial value in classification of hurricanes and in their categorization in terms of maximum wind intensity (Dvorak 1972). Hopefully, the more quantitative SR data, expressed in terms of automatically produced "descriptors," can improve such skills. The accumulation of such a data base has now begun with the preservation of augmented resolution, Mercator-mapped image sections on magnetic tape.

7. OUTLOOK

The immediate need is to expand SR data processing to make better use of the three global coverages available each day--daytime IR data, nighttime IR data, and visual range data. The semi-independent new information available from coincident IR and visual data will lead to a substantial improvement and expansion in the derived product line. It is expected that ambiguities in sea-surface temperatures, which arise in areas of uniform low overcast cloudiness, will be resolved. Similarly, three-dimensional cloud distribution descriptors could be improved. It is also appealing to apply two-channel data to the problems of global energetics. Past efforts in this area have been restricted to lower resolution radiometers than the SR being used for the determination of global patterns in total earth-space energy flux (Winston 1969). Current experiments in the operational mapping of digitized weather radar data offer yet another possibility for application of data combinations (Booth et al. 1972). Mapped afternoon IR responses may provide a more quantitative means of assessing the importance of cloud systems involved in strong radar echo (tornadic) development.

For the longer term, NESS is evaluating the concept of producing a parameterized, quantitative archive based on statistical treatment of SR data clusters, either above or together with other data bases such as the National Meteorological Center's analysis and forecast fields, the Vertical Temperature Pressure Radiometer, and Very High Resolution Radiometer data. The size of the data clusters, geographic grid, and space and time resolution will be determined by experience, user community requirements, and software-hardware limitations. As a first effort in their area, NESS is currently producing a mesoscale data tape as a daily archive. Mesoscale data are compressed from the 2048 x 2048 sample per hemisphere arrays discussed earlier. The data are compressed to a 512 x 512 array of 48-bit words for each hemisphere. The 48-bit words contain SRIR night, SRIR day, and coincident SRVIS data grouped together as indicated in the diagram below.

Average values are calculated as a simple average of the elements in each 4 x 4 cluster obtained from the 2048 x 2048 mapped array. In this way, each hemisphere is reduced from 2048 x 2048 to 512 x 512. The average minimum

Data type	SRVIS		SRIR day		SRIR night*	
Content	$\overline{MN}$	AV	$\overline{MX}$	AV	$\overline{MX}$	AV
No. of bits	8	8	8	8	8	8

*SRIR nighttime data are 12 hours earlier than daytime data

($\overline{MN}$) for SRVIS is an average of the four smallest values in each 4 x 4 cluster. Low values indicate dark or low reflected energy. The average maximums ($\overline{MX}$) for SRIR-DAY and SRIR-NGT are averages of the four largest values in each 4 x 4 cluster. High values indicate warm temperatures. The SRIR values are expressed in the coded temperature scheme listed in appendix C. No data available will be represented by 377 (8).

ACKNOWLEDGMENTS

Special thanks are extended to the professional staff of DAPAD, NESS, especially Mr. J. Anderson, the NESS Photographic Laboratory personnel, and to Mrs. B. Michael and Mrs. E. Shaw, secretaries, without whose help this manuscript could not have been prepared. Particular thanks go to Mr. C. Bristor, who contributed half the narrative and provided additional time and talent in the role of final proof reader.

REFERENCES

Booth, A., DeCotiis, A. G., Leese, J.A., "Automated Procedures for Mapping and Displaying Digitized Radar Data," Proceedings, 15th Conference on Radar Meteorology, Illinois State Water Survey (AMS), Urbana, Illinois, Oct. 1972, pp. 199-203.

Bristor, C. L., "Processing of ITOS Scanning Radiometer Data," Proceedings, 1970 Meteorological Technical Exchange Conference, Hq. Air Weather Service, Scott AFB, Ill., Sept. 1970, pp. 232-242.

Bristor, C. L., Albert, E. G., and Jones, J. B., "Problems in Mapping Data From Meteorological Satellites," Proceedings of Second International Space Symposium, Florence, Italy, North-Holland Publishing Co., Amsterdam, April 1961, pp. 60-70.

Bristor, C. L., Callicott, W. M., and Bradford, R. E., "Operational Processing of Satellite Cloud Pictures by Computer," Monthly Weather Review, Vol. 94, No. 8, Aug. 1966, pp. 515-527.

DeCotiis, A. G., Conlan, E., "Cloud Information in Three Spatial Dimensions Using IR Thermal Imagery and Vertical Temperature Profile Data," Proceedings, Seventh International Symposium on Remote Sensing of the Environment, Center for Remote Sensing Information, Ann Arbor, Mich., 1971, pp. 595-606.

Dvorak, V. F., "A Technique for the Analysis and Forecasting of Tropical Cyclone Intensities From Satellite Pictures," NOAA Technical Memorandum NESS 36, U.S. Department of Commerce, Washington, D.C., June 1972, 15 pp.

Feniger, H., "Data Book, ITOS Scanning Radiometer," Contract Report, Santa Barbara Research Center to Radio Corporation of America, 1969.

Kahwajy, F. T., "Digital Data Handling Systems Equipment Description," NESS Draft Report, Aug. 1970.

Leese, J. A., Booth, A. L., and Godshall, F. A., "Archiving and Climatological Applications of Meteorological Satellite Data," ESSA Technical Report NESC 53, U.S. Department of Commerce, Washington, D.C., July 1970, 125 pp.

Leese, J., Pichel, W., Goddard, B., and Brower, R., "An Experimental Model for Automated Detection, Measurement and Quality Control of Sea-Surface Temperatures From ITOS IR Data," Proceedings, Seventh International Symposium on Remote Sensing of the Environment, Center for Remote Sensing Information, Ann Arbor, Mich., May 1971, pp. 625-647.

Leese, J., Pichel, W., Goddard, B., and Brower, R., "Factors Affecting the Accuracy of Sea-Surface Temperature Measurements From ITOS-SR Data," Proceedings, XVII Annual Symposium on Propagation Limitations in Remote Sensing, AGARD Electromagnetic Wave Propagation Panel, Boulder, Colo., June 1971, pp. 25-1 to 25-13.

McClain, E. P., Baker, D. R., "Experimental Large-Scale Snow and Ice Mapping With Composite Minimum Brightness Charts," ESSA Technical Memorandum NESC TM 12, U.S. Department of Commerce, Washington, D.C., Sept. 1969, 19 pp.

Miller, D. B., et al., "Global Atlas of Relative Cloud Cover 1967-70 Based on Data From Meteorological Satellites," Joint Production of the U.S. Department of Commerce and U.S. Air Force, Sept. 1971, 237 pp.

RCA, Final Engineering Report for ITOS-D, Draft, Undated.

Roth, R. C., "A Data Section Procedure for the Rectification and Mapping of Digitized Data," Technical Memorandum AFGWC 69-1, Air Weather Service, Offutt AFB, Neb., Dec. 1969, 20 pp.

Ruff, I., Koffler, R., Fritz, S., Winston, J.S., and Rao, P. K., "Angular Distribution of Solar Radiation Reflected From Clouds As Determined From TIROS IV Radiometer," ESSA Technical Report NESS 38, March 1970, 20 pp.

Schwalb, A., "Modified Version of the Improved TIROS Operational Satellite (ITOS D-G)," NOAA Technical Memorandum NESS 35, U.S. Department of Commerce, Washington, D.C., Apr. 1972, 48 pp.

Smigielski, F. J., Mace, L. M., "Estimating Mean Relative Humidity From the Surface to 500 Millibars by Use of Satellite Pictures," ESSA Technical Memorandum NESC TM 23, U.S. Department of Commerce, Washington, D.C., Mar. 1970, 12 pp.

Smith, W. L., Rao, R. K., Koffler, R., and Curtis, W. R., "The Determination of Sea-Surface Temperature From Satellite High Resolution Infrared Window Radiation Measurements," Monthly Weather Review, Vol. 98, No. 8, Aug. 1970, pp. 604-611.

Taylor, V. R., "Operational Brightness Normalization of ATS-1 Cloud Pictures," ESSA Technical Memorandum NESS TM 24, U.S. Department of Commerce, Washington, D.C., Aug. 1970, 15 pp.

Winston, J. L., "Global Distribution of Cloudiness and Radiation As Measured From Weather Satellites," World Survey of Climatology, Vol. 4 (Climate of the Free Atmosphere), Chapter 6, Elsevier Publishing Co., Amsterdam, Holland, Aug. 1969, pp. 247-280.

APPENDIX A. NOTES ON THE INGESTION OF NOAA-2 RECORDED SR DATA

1. DEFINITION OF DATA

Figure 13 and tables 4 and 5 define ITOS-D SR data. The following additional comments further define and clarify the NOAA-2 SR data (recorded) as received and digitized at NESS.

A. The order in which recorded data are received at NESS is opposite that shown in figure 1, i.e., the sync pulse will precede the telemetry window, which immediately precedes the earth scan, etc. The time periods shown should be divided by 5.2--the effective speedup from recording on the satellite to playback to NESS.

B. Table 4 defines the SR data stream for an individual scan line; 25 scans define a frame (table 5). The 600-Hz marker will be used at NESS to indicate the beginning of a frame. This marker, coupled with the reverse direction on playback, generated the following comparison:

Ingested scan no. of a frame	Data frame scan no.
1	2
2	1
3	25
4	24
24	4
25	3

C. Note that telemetry contained in channels 21-23 and 25 of the visible data is information that can be used in calibrating the IR data. This fact is considered in the output tape format and will be shown under that section.

D. The digitization and outputting of recorded SR data at NESS will yield 8-bit samples whose values are low for IR hot and visible white, and high for IR cold and visible black.

2. INGEST MODES

The visible data are sampled at the same rate as the IR data (58-sec sampling period) in lieu of the differences in resolution. Furthermore, the data (IR and VIS) will normally be written on separate nine-track tapes.

However, the SR ingester will have the flexibility of changing this normal mode by means of an operator type in. A mode number will be placed in the header record(s) on tape(s) and will be coded as follows:

Mode no. (base 8)	
0	- "Normal Mode" - The VIS is sampled at the same rate as the IR. IR and VIS WRITTEN ON SEPARATE 7-track tapes.
1	- The VIS is sampled in 29 sec, or twice the IR rate, IR and VIS written on separate 7-track tapes.
2	- VIS rate = IR rate. IR written on 7-track. VIS written on 9-track.
3	- VIS rate = 2 x IR rate. IR on 7-track. VIS on 9-track.
4	- VIS rate = IR rate. IR on 9-track. VIS on 7-track.
5	- VIS rate = 2 x IR rate. IR on 9-track. VIS on 7-track.
6	- VIS rate = IR rate. IR and VIS written on separate 9-track tapes.
7	- VIS rate = 2 x IR rate. IR and VIS written on separate 9-track tapes.
10	- VIS rate = IR rate. IR and VIS combined on 7-track tape.
11	- VIS rate = 2 x IR rate. IR and VIS combined on 7-track tapes.
16	- VIS rate = IR rate. IR and VIS combined on 9-track tape.
17	- VIS rate = 2 x IR rate. IR and VIS combined on 9-track tape.

3. PRELIMINARY TAPE FORMAT FOR RECORDED ITOS-D SR

A. First Record(s)

The first record of every tape utilized for the ingestion of ITOS-D recorded SR will be 45 16-bit words of the following format:

word 3 - Readout orbit number

words 6 - 8 - Satellite Name (6 EBCDIC Characters)

words 11 - 12 - NASA reference time for reset of 24-bit spacecraft counter

word 11

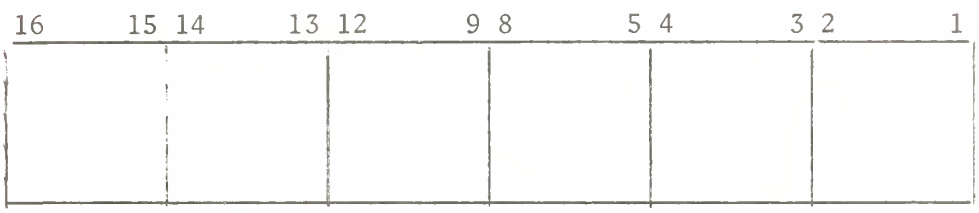

Undefined	Hundreds of days	Tens of days	Units of days	Tens of hours	Units of hours

word 12

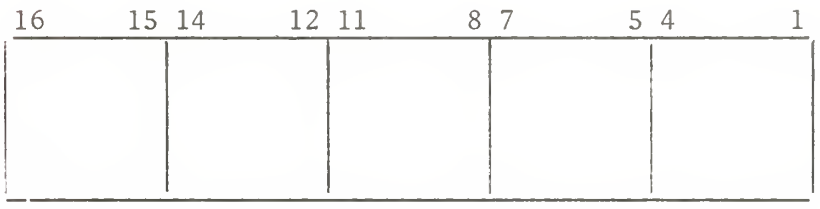

Units of hours	Tens of minutes	Units of minutes	Tens of seconds	Units of seconds

word 15 - Readout station

0 = Gilmore

1 = Wallops

word 18 - Mode of ingest (as defined in ingest modes of attached notes)

word 21 - Tape number (1,2, etc.)

All other words within this record are undefined at this time.

B. Digitized SR Data Records

All SR data records will be 1830 16-bit words. In the normal case where visible is sampled at the same rate as the infrared, this record will contain two scans of IR, or (exclusive) VIS plus documentation. Fifteen words of documentation are used for each scan. The format follows:

words 1 - 15 - 15 words documentation

words 16 - 915 - 900 words digitized data

words 916 - 930 - 15 words documentation

words 931 - 1830 - 900 words digitized data

2nd documentation word - frame count

4th documentation word - line number (1-25)

6th documentation word - identification

77777_8 for VIS

33333_8 for IR

8th documentation word - error indicator for previous frame. If #0, this indicates previous frame out of sync.

If line number = 3 (4th Doc. word), the 10th and 11th documentation words contain the spacecraft 24-bit time count. This count corresponds to the time of the previous scan (line number 2). The most significant bit indicated by bit 8 of the 10th word and the least significant bit by bit 1 of the 11th word. If the time count = 0, the ingester was unable to decode the time. Bit 16 of word 10, when set, indicates that only the least significant 16 bits of the time count is given (in the 11th word).

The 15th documentation word of IR lines 3, 5, 6, and 7 will, respectively, contain the following 20 sample averages of telemetry.

IF IR line = 3, 15th Doc. word = average reference "black body" temperature.

IF IR line = 5, 15th Doc. word = average reference "black body" temperature.

IF IR line = 6, 15th Doc. word = average of electronics module temperature.

IF IR line = 7, 15th Doc. word = average of scanner electronics temperature.

Immediately following the 15-word documentation are the 900 words of digitized data. Nominally, in order, there will be:

17 words of sync backporch

83 words of digitized telemetry

100 words of space view

621 words of earth view

79 words of space and sync

C. Visual Data Format at Twice the Normal Rate

If visible data are sampled at twice the rate (odd numbered ingest modes), one visible scan will be written per 1830-word record in the following format:

Word 2 - frame count

Word 4 - line number (1-25)

Word 6 - ID of 44444_8

Word 8 - error indicator as defined in normal case

If line number = 3, words 10 and 11 contain the time count as defined in the normal case.

Words 16 - 1815 - The digitized data. Nominally, in order, there will be:

34 words of sync backspace

166 words of digitized telemetry

200 words of space view

1242 words of earth view

158 words of space 8 sync

Words 1816-1830 - undefined

D. End-of-Ingest/End-of-File

An end-of-ingest will be indicated by a 45-word quality control record (written on both tapes if IR and VIS are written on separate tapes). The quality control information is undefined at this time.

An end-of-file will indicate no more useful data on this tape. Thus an end-of-file not preceded by the 45-word record indicated that other tapes were subsequently used.

Table 4.--*SR data timing, SRPR output*

	Function	Time after start of IR real-time sync (milliseconds)	Duration (milliseconds)	Characteristics real-time signal modulated 2,400 Hz subcarrier	Characteristics of playback signal (demodulated)
1.	Real-time synchronization (real time only)	0.0	23.31	Seven pulsed 300 Hz square wave 100% amplitude.* Starts at 68°±2° before nadir.	4% amplitude
2.	Space scan pre-earth (IR)	23.31	24.47†	96% Amplitude*	Continuation of above
3.	Earth scan (IR)	47.78†	377.78†	Period varies, from 364 mscc @ 900 n mi to 406 mscc @ 000 n mi. Dynamic range 4% to 96% amplitude	Same as real-time signal. Cold targets approach 4%** level, hot targets near 87%** level.
4.	Space scan post-earth (IR)	425.56†	61.11†		Same as real-time signal.
5.	Telemetry Window #1	486.67±3.0††	50±3.0††	Voltage calibration function as shown	Function shown is voltage calibration. Function telemetered changes with successive scan line, see table 7 for details.
6.	Back porch	536.67±6.0††	10±1††	Amplitude* 100% level	Amplitude** 0% level
7.	Playback synchronization	546.67±7.0††	30±2††	Minimum amplitude	Pulse amplitude** 100% approximately 11.5% higher than other signals.
8.	Front porch	576.67±9.0††	10±1††	Amplitude* 100% level	Amplitude** 0% level
9.	Back scan	586.67	10.73		Same as real-time signal

10.	Data overlap	597.40	12.50		IR back scan contaminated by VIS back scan
11.	Sync delay	609.90	15.10	DC restore followed by space scan	Same as real-time signal
12.	Real-time synchronization (VIS)	625.00	23.31	Same as IR signal	Same as IR real-time signal
13.	Space scan pre-Earth (VIS)	648.31	24.47†	4% amplitude	87% amplitude
14.	Earth scan (VIS)	672.78†	377.78†	Period varies identically with IR Earth scan. Dynamic range 4% to 100% amplitude.	Same as real-time signal, bright clouds approach 4% level,** black is 90% level.**
15.	Space scan post-earth	1050.56†	61.11†		Same as real-time signal
16.	Telemetry Window #2	1111.67±3.0††	50±3††	See table 7 for details.	Same as real-time signal
17.	Back porch	1161.67±6.0††	10±1††	Amplitude* 100% level	0% amplitude**
18.	Playback synchronization (VIS)	1171.67±7.0††	30±2††	Minimum Amplitude* (2 to 4%)	100% amplitude
19.	Front porch	1201.67±0.0††	10±1††	Amplitude* 100% level	0% amplitude
20.	Back scan	1211.67	10.73		Same as real-time signal
21.	Data overlay	1222.40	12.50		VIS back scan contaminated by IR back scan
22.	Scan delay	1234.90	15.10	DC restore followed by space scan	Same as real-time signal
23.	Real time (IR)	1250.00		Same as Number 1	

*Full amplitude is taken as the amplitude of front and back porch. †At spacecraft altitude of 790 n mi.

**Full amplitude of playback signal is the playback sync pulse. ††Tolerance within the scanning radiometer

Table 5.--*SR telemetry window data*

Scan line[1] number	No. 1 window IR portion recorded data[2]	No. 2 window visible portion both real time and recorded
1	Spacecraft time code (16 least significant bits)	Spacecraft time code (16 most significant bits)
2	100-Hz marker	600-Hz marker
3	0.0-volt calibration	0.0-volt calibration
4	-5.0-volt calibration	-5.0-volt calibration
5	SR no. 1 identifier (-5 V) or SR no. 2 identifier (0 v)	Housing backscan (sampled)
6	Housing backscan (sampled)	Spare
7 through 20	Voltage calibration steps[3]	Voltage calibration steps[4]
21	SR housing ref. A temperature	Scanner electronics temperature
22	IR detector temperature	Electronic module temperature
23	SR housing ref. B temperature	SR housing ref. C temperature
24	Spare	Spare
25	IR detector bias	SR housing ref. D temperature

[1]Numerical order is for real-time data. Playback data are presented in reverse order.

[2]In the real-time data, voltage calibration occurs on every scan.

[3]Part of IR signal from SR electronics.

[4]Part of VIS signal from SR electronics.

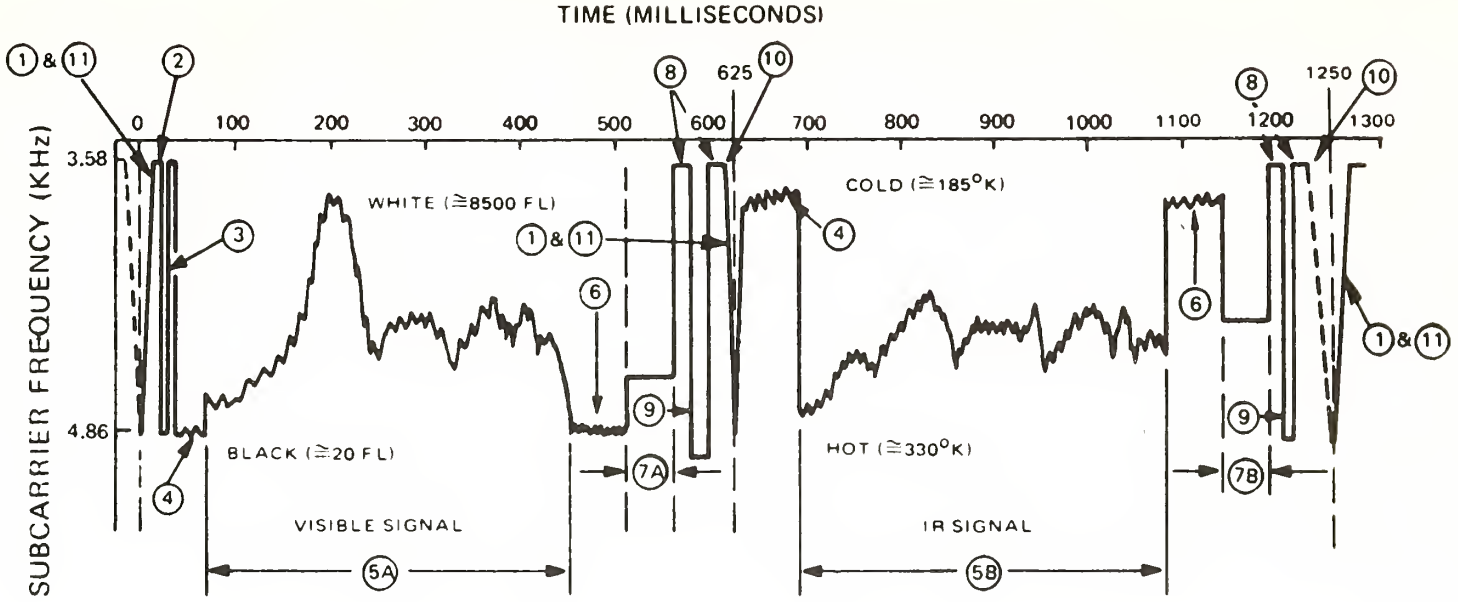

1	IR & VIS DATA OVERLAP	12.5 MILLISECONDS
2	SYNC BURST DELAY	15.1 MILLISECONDS
3	LINE SYNC TONE BURST (300 Hz)	23.3 MILLISECONDS VIS, 38.4 MS IR
4	OUTER SPACE SCAN	24 MILLISECONDS
5	EARTH SCAN A. VISIBLE	378 MILLISECONDS
	B. IR	378 MILLISECONDS
6	SPACE SCAN	61 MILLISECONDS
7A	VIS TELEMETRY CHANNEL PERIOD	50 MILLISECONDS
7B	IR TELEMETRY CHANNEL PERIOD	50 MILLISECONDS
8	FRONT & BACK PORCH	10 MILLISECONDS, EACH
9	SYNC PULSE	30 MILLISECONDS
10	BACK SCAN	10 MILLISECONDS
11	HEAD SWITCHING TRANSIENT	2 MILLISECONDS

Figure 13.--*Recorded SR signal characteristics after time multiplexing by SR recorder (time and frequency values shown for record mode)*

APPENDIX B: CALIBRATION PROCEDURES

1. INFRARED CHANNEL CALIBRATION PROCEDURE

The calibration of the ITOS scanning radiometers is a two-step procedure that is applied in real time to the tape recorded data stream. For ease of discussion, step 1 is termed electrical calibration and step 2 thermal calibration.

Electrical calibration information makes it possible to correct for nonlinearities introduced into the NESS received analog data as it proceeds through the data path from radiometer to NESS. The data path consists of the spacecraft electronic-recorder system, transmission links--both atmospheric and longline, and ground station equipment. At the heart of the electrical calibration is a simple, but stable, circuit that generates six predetermined voltage levels which are introduced into the SR data path. Upon receipt at NESS, the outputs for the generated signals are compared with their linear, pre-launch counterparts. If significant nonlinearity exists, a least-squares curve of up to third order is fitted to the new data, relating output and generated voltage. A chi-square goodness-of-fit test is used to choose the order curve used for the fit. A transformation equation is then determined from the equations of the pre-launch and in-flight curves. All real-time outputs are then passed through the transformation algorithm. When all data are transformed, the electrical calibration is complete.

Thermal calibration is based on the following considerations:

a. The radiometers are linear with energy over the range of normal spacecraft operating temperatures and the range of scene temperatures viewed during flight.

b. The radiometer regularly views an onboard reference "black body" of known temperature during flight. In practice, the black body temperature is telemetered and inserted in the data stream.

c. Deep space is essentially a radiative constant over the radiometer bandpass and is regularly viewed by the radiometer during flight shortly before the instrument views the reference black body.

d. The radiometer's relative response function is known from laboratory measurements.

Given the above, thermal calibration is affected by relating the sensor output, C, to incident energy, N, over the sensor bandpass to the equivalent black body temperature, T, of the viewed scene as filtered by the sensor system. Analytically, the procedure is defined by

$$N(T) = \int_{\lambda} B(\lambda,T)\phi(\lambda)d\lambda \qquad (1)$$

and

$$N(T) = mC+b \qquad (2)$$

where N(T) is the bandpass weighted energy, $B(\lambda,T)$ is the Planck Function, $\phi(\lambda)$ the relative response function, C the radiometer output when looking at a scene of equivalent black-body temperature T, and m and b are calibration parameters calculated during processing. The value of m is given by

$$m = \frac{N(T_{BB}) - N(T_{SP})}{C_{BB} - C_{SP}} \tag{3}$$

where $N(T_{BB})$ is obtained from eq (1) evaluated for the known, reference black body temperature, and $N(T_{SP})$ is the energy value given by eq (1) when evaluated for 3.5°K, the generally accepted radiative temperature of deep space; however, in practice $N(T_{SP})$ is taken as zero energy. C_{BB} is the radiometer output when viewing the onboard black body at the temperature T_{BB}, and C_{SP} is the radiometer output when it views deep space. Having evaluated m, the value for b is obtained by substitution in eq (2); when viewing space, N(T) is zero; therefore

$$0 = m\ Csp + b \tag{4}$$

and it follows that

$$b = -m\ Csp \tag{5}$$

Substituting the values obtained for m and b from eq (3) and (5) in eq (2), radiometer outputs are converted to energies, $N(T)_i$, that are in turn converted to equivalent black body temperatures by inverting eq (1).

A final correction to the temperature is then applied to correct for instrument bias if the laboratory test data show it is necessary. This completes the thermal calibration.

2. VISIBLE CHANNEL CALIBRATION PROCEDURE

As with the thermal channel, the calibration of the visible channel is a two-step procedure. Again, step 1 is the electronic calibration performed as for the IR channel, and step 2 is a brightness calibration by which energy in the 0.52 to 0.72-um region is converted to foot-lambert units.

Laboratory measurements serve as the basis for the brightness calibration. Prior to launch, visible channel outputs are measured when the radiometer is looking at a brightness source of known foot lamberts. The brightness source is a quartz iodide bulb viewed through an external filter. Bulb and filter combine to cause the radiometer to see an equivalent brightness

compatible with the sun's color temperature. A curve is then fitted relating the radiometer output and the solar equivalent brightness measurements. This curve is essentially linear and is the calibration algorithm.

Thermal Channel Atmospheric Attenuation Correction

Although the 10.5- to 12.5-um region is known as the "window channel" for longwave radiation, it is known that radiation emitted by the earth and clouds in this spectral band is slightly attenuated by the atmosphere. The principal absorbers in this region are water vapor (the most important), carbon dioxide, and ozone. The extent of attenuation is a function of their concentrations in the radiometer field of view. In theory, if the concentration, as a function of pressure and temperature, were known, NOAA 2 satellite observations could be corrected for their effects. However, this information is not usually known well enough to permit accurate, quantitatiave evaluation on a near real-time global basis.

In spite of the difficulties, an attempt is made to partially correct the ITOS observations for atmospheric effects. Since the attenuation is related to the radiometer field of view, and because the radiometer is a scanning device, the total attenuation can be divided into two components. One is the attenuation when the radiometer points straight down and the second is the contribution added by increased path length when the sensor points to a target at some angle away from the straight down position.

Of the two components, the straight down component is dominant. An unpublished NESS analysis of over 100 model atmospheres shows the total attenuation to be equivalent to a temperature difference of up to 9°C in the 300°K range. This amounts to a possible error of more than 3%--an unacceptably large value if the NESS tried to correct statistically for the effect. On the other hand, the same analysis indicates a probable error of not more than 1% when the angular attenuation contribution is treated statistically. This correction is applied during the data processing.

In practice, the statistical angular correction is expressed as a function of the uncorrected, observed equivalent black body temperature and satellite viewing angle. In effect, the inclusion of the observed temperature in the functional relation gives a coarse approximation of the temperature-pressure state of the absorbers. The net effect is to correct all observations to represent the expected attenuated measurement that would be obtained if the radiometer viewed the target in the straight down position. It is left to the user to provide his own estimate of the straight down correction except in the case of derived sea-surface temperatures. In this case, plans call for using the Vertical Temperature Profile Radiometer (VTPR) data to effect the necessary correction (appendix E).

3. SUN NORMALIZING

In simple terms, sun normalizing is the process by which the radiometer visible channel output is corrected so reported measurements are the same when viewing a given target, regardless of target location, time of day, or

viewing angle. Experience has shown that the necessary correction factor is strongly dependent upon three angles and the reflective characteristics of the target. The angles are the zenith angles of the sun and satellite relative to the target, and the angle between the sun and satellite, measured clockwise from the target; however, since a satisfactory algorithm for solving the three-angle model is not available, NESS uses a simple one-dimensional model involving the cosine of the solar zenith angle. The Meteorological Satellite Laboratory of NESS is working on a solution to the three-angle model.

4. CALIBRATION NOISE ERRORS IN CALIBRATED SCANNING RADIOMETER INFRARED DATA

The basic calibration equation that relates the scanning radiometer output to input energy is

$$E = m(C - C_{sp}) = m\Delta C \tag{6}$$

where E is input energy, m the slope of the linear relationship and a value derived during the calibration procedure, C the digitized sensor output for an arbitrary field of view, and C_{sp} the digitized output when the radiometer looks at space--an essentially zero energy source.

Looking again at eq (6), calibration noise errors arise in the determination of the slope, m. For the case when a noise-induced error is included in m, eq (6) becomes

$$E = (m + \Delta m)(C - C_{sp}) = (m + \Delta m)\Delta C \tag{7}$$

where m is the noise-induced error in m.

Subtracting (6) from (7) gives

$$\Delta E = \Delta m(C - C_{sp}) = \Delta m \Delta C \tag{8}$$

From analytic geometry

$$m = \frac{\Delta E}{\Delta C} \qquad \frac{E_{BB} - E_{SP}}{\Delta C} = \frac{E_{BB}}{\Delta C} \tag{9}$$

where E_{BB} is the energy emitted by a reference source of known temperature, and E_{SP} the energy of space, taken as zero as stated earlier. Differentiating m with respect to E_{BB} and ΔC and substituting finite approximations for total derivatives gives

$$\Delta m = \frac{\partial m}{\partial E_{BB}} \Delta E_{BB} + \frac{\partial m}{\partial \Delta C} (\Delta C). \tag{10}$$

From eq (9)

$$\frac{\partial m}{\partial E_{BB}} = \frac{1}{\Delta C} \tag{11}$$

if only noise errors are considered and

$$\frac{\partial m}{\partial \Delta C} = \frac{-E_{BB}}{(\Delta C)^2} = \frac{-m}{(\Delta C)} \tag{12}$$

Equations (11) and (12) allow (10) to be written as

$$\Delta m = \frac{1}{\Delta C}\Delta E_{BB} + \frac{(-m)}{\Delta C}\Delta(\Delta C) \tag{13}$$

Analysis of the RMS noise of the communications-digitizing system shows it to be 3.0 counts. Since two different count measurements are used in the construction of ΔC, the worst-case value is 6 counts. Further, if we consider the 95% worst situation in each value there can be a difference of 18 counts. However, in the operational processing mode, 2,000 samples of C_{BB} and 20,000 samples of C_{SP} are averaged before being used in the computation of m; therefore, $\Delta(\Delta C)$ is less than 0.14 in eq (13). A similar analysis gives an error of less than 0.3 counts in the value used for computation of ΔE; however, the absolute resolution RMS of the devices used to measure the temperature of the reference source involved in the calculation of m is 0.5°C. The two effects combined at the 95% worst level, to give a maximum error of 100 erg units for a temperature near 290°K. In reality, the count-induced error is so small it can be disregarded in further computation.

Rewriting eq (13) in view of the foregoing yields

$$\Delta m = \frac{1}{\Delta C}(100) + \frac{(-m)}{\Delta C}(0.14) \tag{14}$$

Drawing on experience with the ITOS and NOAA 1 satellites in the normal operating mode,* $1/\Delta C$ can be estimated as -1/125 and m as -90. Substituting these values in eq (14) gives:

$$\Delta m = \frac{-100}{125} + \frac{(-90)}{125}(0.14) = -0.9 \tag{15}$$

From eqs (8) and (15)

$$\Delta E = 112$$

for temperatures in the neighborhood of 290°. This value equates to 0.8°C in terms of temperature. However, the 0.8°C error occurs only when the three

*m and ΔC are both functions of the spacecraft thermal configuration. Estimates for nonnormal operating modes can be determined from the prelaunch calibration information.

variables affecting m are all adversely arranged, each at the 95% level. Thus, in practical terms, this magnitude error occurs at the 0.01% level if we assume that noise-induced calibration errors form a normal distribution. Given this, the RMS error, in terms of temperature, is 0.3°C.

Prelaunch laboratory tests of the radiometer and experience with ITOS-1 and NOAA-1 radiometers show that the overall system RMS noise is about 2°K in the neighborhood of 290°C. This effect must be added to the calibration noise. This done, the total RMS calibration noise error is 2.02°C.

APPENDIX C: DESCRIPTION OF SR PRODUCTS

1. SR-IR 360° COVERAGE

This segment establishes the processing sequence, input, normalizing, and calibrating of the raw source SRIR data from digital tape. The typical input volume for a complete global circle is 225 frames of 25 scans each. On completion of this segment the data for both mapping and sea surface temperature (SST) computation reside in disk storage for processing by any of the following segments.

a. 2048 Polar day - IR (2 Hem): Global mapping segment for ascending node (daytime) SR data. The data from the ascending portion of the orbit are composited to a polar stereographic map projection with 2048 x 2048 map points per hemisphere with the North Pole coordinate (1024, 1024) and pole coordinate (1024, 3072). This array has a spacial resolution of 4 mi at the equator and 8 mi at the pole. The data are mapped as 8-bit quantities.

b. 11.25 Mercator Nite - IR: The ascending node SR data are mapped to a Mercator projection scaled to have 11.25 map points per degree of longitude. This provides an effective resolution of 5 mi at the equator, increasing with latitude. The map coverage is for 360° longitude, from 40°N to 40°S latitude, providing for an array of 4050 columns by 984 rows. The data are mapped as 6-bit quantities.

c. Pass/Pass Nite polar - IR: Ascending node data are mapped to a polar stereographic map projection in a 2048 x 2048 array in such a manner that the node longitude is orthogonal horizontally to the map array. The array dimensions are 1020 columns by 408 rows, providing latitude coverage from the pole to the equator horizontally and, vertically, 25° longitude at the Equator. The data are mapped as 6-bit quantities.

d. APOLM N. Pole: Augmented resolution mapping of SR data to a polar stereographic map projection with 4096 x 4096 map points per hemisphere. The resolution is 2 mi at the Equator and 4 mi at the pole. The limited area array is 896 columns by 512 rows. The data are mapped as 6-bit quantities. The 6-bit compression from source 8-bit quantities is a function of an alterable lookup table read from cards during program load. The day/night partition can be ignored in the mapping. The geographic placement of the 896 x 512 array is variable as a function of center point latitude, longitude, and orthogonal prime longitude.

e. APOLM S. Pole: Identical in format to APOLM N. Pole, except located over Antarctic.

f. APOLM U.S. Nite: Ascending SR-IR composited into 896 x 512 augmented array as described in item 1.d and located over the United States.

g. AMERM 16.0 Mercator: Augmented resolution mapping of SR data to a Mercator map projection having a resolution of 16 array points per degree of longitude. This provides for a map resolution of 4 mi at the equator and greater with increasing latitude. The map array limits are 357 columns by

408 rows for geographic coverage about 22° square. The geographic placement of the augmented array is a function of input variables designating center point latitude and longitude. The choice of ascending or descending IR, or VIS data is a function of a variable input from a data card.

h. FAXOUT pass/pass: Output of pass/pass polar mapped SR data (see item 1.c above) for standard 120-line facsimile transmission. Product includes gray scale wedge and latitude-longitude grid overlays. The map array is expanded by a factor of 2.25 so the resulting array output on a standard 18-inch Alden facsimile will fit a 1:20M map scale. The labeling is repeated on top and bottom, and left and right halves so the product can be easily reformatted for broadcasting in the WEFAX or APT mode.

i. DMD pass/pass: Output of pass/pass polar mapped SR (see 1.c above) for Muirhead D-700 photo recording in the 2500 mode. A gray scale precedes the output array.

j. SST (sea surface temperature): Global sea-surface temperature values are accumulated on a 512 x 512 hemisphere map array. Values are computed only for those map points over ocean areas.

2. SR-VIS 180° COVERAGE

This segment is required to establish processing sequence and input, and solar illumination correcting and calibrating of the raw SR-VIS data from digital tape. The typical input volume for the daylight portion of the orbit is 225 frames of 25 scans each. The following processing segments require the data formatted by this segment:

a. 2048 Polar VIS: Global mapping segment for descending node visible data. The format is identical to that for the 2048 x 2048 mapping of SR-IR data. See 1.a and table 5.

b. 11.24 Mercator VIS: The descending node SR-VIS data are mapped to a global Mercator map array in a configuration identical to that for the IR Mercator data (1.b).

c. Pass/pass Polar VISIBLE: Descending node VIS data mapped to a single pass polar array. Identical to the SR-IR pass-by-pass array (1.c).

d. APOLM U.S. VISIBLE: A composite of descending node data mapped in augmented polar form as for the IR in 1.d.

e. AMERM 16.0 Mercator VISIBLE: Augmented Mercator coverage for VIS as for IR in 1.g.

f. FAXOUT pass/pass: Same format as in 1.h.

g. DMD pass/pass: Same format as in 1.i.

3. OUTPUT/ARCHIVE PRODUCTS

The products listed below are run in support of all those functions listed under 1 and 2.

a. IR WEFAX via ATS-1: The SR-IR data mapped to Mercator (1.b) and polar projections (1.a and 1.b) are formatted for transmission in the WEFAX or APT mode via the transponder on ATS-1.

b. IR WEFAX via ATS-3: The SR-IR data mapped to Mercator (1.b) and polar (1.c) projections are formatted for transmission in the APT mode via ATS-3.

c. 2048 Polar DMD: The polar mapped SR data (1.a and 2.a) are formatted for display on the Muirhead D-700 photo recorder attached as part of the DMD system. The display scale and latitude correction, where necessary, are parameters input from data cards. The source input for this operation is the 2048 polar archive tape. The product is displayed on the D-700 as a single hemisphere per film chip run in the 2500 mode.

d. 11.25 Mercator DMD: The Mercator mapped SR data (1.b and 2.b) are formatted for display on the Muirhead D-700 system. A single film chip produced in the 2500 mode contains two 180° segments. The display scale is input as data card parameters.

e. APOLM DMD: The augmented polar chip data (1.d, e, f, and 2.d) are formatted for output to Muirhead D-700 display. A gray scale wedge, and latitude, longitude, and geographic outline are added to the product.

f. AMERM DMD: The augmented Mercator chip data (1.g, 2.e) are formatted for output to Muirhead D-700 display. A gray scale wedge, and latitude, longitude, and geographic outline are added to the product.

g. Double 2048 Archive: The ascending SR-IR and SR-VIS data are archived on magnetic tape as 8-bit quantity couplets forming a 16-bit byte for each of the 2048 x 2048 map positions. Each hemisphere requires a separate digital tape archive.

h. 11.25 Mercator 1:20M Fax: The Mercator mapped SR data (1.b, 2.b) are formatted for transmission over standard facsimile circuits at 120 lines per minute. Each chip is provided a 1:20 million map scale for the product when displayed on an 18-inch Alden facsimile. The coverage for each chip displayed is from 40°N to 30°S and for 80° longitude.

i. Predictive Grids: The overlay grids for melding with SR and APT are predicted for a 48-hr period to provide for continuous gridding capability. Similar gridding capability will be processed for the SR products.

j. Unmapped DRIR DMD: The DRIR data are formatted for display on the Muirhead D-700 in unmapped form. The image is displayed in duplicate form allowing for variable tone shading to depict different features in each of the two halves.

APPENDIX D: EARTH MAPPING OF SCANNING RADIOMETER DATA

The earth location logic package at NESS is designed to calculate latitude and longitude values for each scan element along each scan input from the satellite. However, solution of the complex spherical geometry required for computing these coordinates involves excessive computer cycles, making such computation uneconomical. Below is an explanation of the algorithm used to make this process more efficient.

a. Computer economics can be improved significantly if coordinates are computed for only a selected number of scan elements so as to form a network of values for an open lattice matrix. This permits computation of intermediate scan element coordinates through an interpolation algorithm.

b. The interpolation algorithm chosen is one that maintains mapping integrity but yet is economical for computer processing. The incoming analog signal must be digitized, and the maximum digitizing accuracy is plus or minus an increment the size of a viewed spot. For example, a view sample having a resolution of 2 mi can be inaccurate by as much as 4 mi. Therefore, mapping integrity demands that the interpolation scheme must provide accuracy to within the inherent accuracy of the digitizing process. Logically, one would assume that a second- or third-order interpolation would meet this requirement. However, second- and third-order interpolations are costly in terms of computer cycles. An alternate scheme for linearly interpolating intermediate values was developed to increase the economy of computing coordinate values for the individual samples. This logic is critically dependent on the separation of reference values called benchpoints, between which the individual coordinate values are to be calculated. When operating with linear interpolation to calculate values spread over a curved surface, the benchpoint separation increment must be such that the straight line segment connecting the bench marks does not deviate from the real segment by a factor larger than the inherent sample accuracy. The separation of benchpoint calculations is selected as a function of

$$\Delta I = \frac{B_{M+1} - B_M}{I}, \text{ and}$$

$$S = BM + \sum_{1}^{MR} \Delta I$$

This process is repeated for every earth-located sample. The ΔI quantity is computed only once for each benchmark interval to conserve computer cycling.

APPENDIX E: INTERFACE OF VTPR ATMOSPHERIC WATER VAPOR MEASUREMENTS AND SR SEA-SURFACE TEMPERATURE DATA

Starting with the ITOS-D satellite, the onboard sensor package will include a multi-channel Vertical Temperature Profile Radiometer (VTPR) and a two-channel (infrared and visible) scanning radiometer (SR). Data from the VTPR instrument will provide indirect measurements of atmospheric temperature and humidity profiles, while the infrared channel of the SR instrument will provide measurements in the atmospheric window region.

An interface has been established between the VTPR and SR sea-surface temperature (SST) models to exchange SR clear column radiance data and the VTPR atmospheric water vapor field. The VTPR model uses the latest sea-surface temperature field as a baseline to determine clear column radiance needed for reduction of VTPR data. In turn, the SR sea-surface temperature model uses the VTPR atmospheric water vapor measurements to compute necessary atmospheric attenuation corrections.

Attenuation corrections are then applied to the sea-surface temperature retrievals during the mapping phase of the data processing.

Eq. (16) is used to calculate the sea-surface temperature, T_s.

$$T_s = T_e\ (\Theta) + A'\ \mathrm{Sec}\ \Theta + B'\ \mathrm{Sec}^2\ \Theta, \qquad (16)$$

where T_e is the equivalent black body temperature retrieved by the SR instrument, A' and B' are water vapor attenuation coefficients derived from the VTPR measurements, and Θ is the viewing angle measured at the satellite nadir angle.

The coefficients A' and B' are evaluated using the following technique:

Compensation for atmospheric attenuation in the nadir direction is given by

$$\Delta T_{SR} = T_{SR} - T_{SFC} = \Delta T_{VTPR} + (T_{VTPR} - T_0)\ C \qquad (17)$$

where ΔT_{SR} is the atmospheric correction to be applied to the SR measurements, ΔT_{VTPR} is the calculated correction for the 835-cm^{-1} channel of the VTPR instrument, and T_0 and C are constants calculated for the particular instrument used. Values of T_0 and C are determined by calculating equivalent black body (EBB) temperatures for both instruments for a number of atmospheres, plotting the differences in calculated EBB temperatures ($T_{SR} - T_{VTPR}$) as a function of T_{VTPR}, and fitting a straight line through the resulting points. Values of the quantity $(T_{VTPR} - T_0)C$ range from 0.2° to 0.8°K for values of T_{VTPR} near 300°K, and approach zero for values of T_{VTPR} near 270°K. After the satellite is launched, values of T_0 and C will be checked by comparing measurements of T_{SR} and T_{VTPR} over clear areas.

The angular dependence of the atmospheric correction is also calculated from the VTPR measurements. Values of ΔT_{VTPR} are calculated from the temperature and humidity profiles derived from VTPR measurements for zenith angles of zero and 60 degrees. An additional value is known since ΔT_{VTPR} must be zero when τ is equal to zero. These three points result in values of $\tau \sec \theta$, of 0, τ, and 2τ, where τ is atmospheric transmittance.

A parabola is fitted to the three points of ΔT_{VTPR} versus $\sec \theta$, resulting in values of A and B given by

$$\Delta T_{VTPR}(\theta) = \Delta T_{VTPR}(\theta = 0)[A \sec \theta + B \sec^2 \theta], \tag{18}$$

which leads to

$$B = -1.0 + 0.5\Delta T_{VTPR}(\theta = 60)/\Delta T_{VTPR}(\theta = 0) \tag{19}$$

and

$$A = 1.0 - B \tag{20}$$

To obtain the angular dependence of T_{SR}, values of A and B for the SR instrument are assumed to be equal to the values derived for the VTPR instrument. The final correction is then given by

$$\Delta T_{SR}(\theta) = [\Delta T_{VTPR}(\theta = 0) + (T_{VTPR} - T_0)\, C]\, [A \sec \theta + B \sec^2 \theta] \tag{21}$$

which for a given atmosphere reduces to

$$\Delta T_{SR}(\theta) = A' \sec \theta + B' \sec^2 \theta, \tag{22}$$

where A' and B' are given by

$$A' = [\Delta T_{VTPR}(\theta = 0) + (T_{VTPR} - T_0)\, C]\, A \tag{23}$$

$$B' = [\Delta T_{VTPR}(\theta = 0) + (T_{VTPR} - T_0)\, C]\, B. \tag{24}$$

Schedules, data handling errors, and mechanical failures can cause the loss of the time-synchronous orbits of the VTPR and SR data pairs. In the event of any such loss of VTPR data, a dual backup system has been designed into the SST model. System 1 incorporates a daily mapping of all attenuation coefficients into a coarse-grid polar stereographic grid field. Data in this field are maintained for 72-hr periods on a latest available data replacement basis. Thus, in the event of loss of the coincident orbital data, the attenuation compensation coefficients will be extracted from this backup field. If data in the backup field should be older than 72 hr, as would occur with failure of the VTPR instrument, the attenuation correction would be derived from an empirical average correction lookup table.

☆ U. S. GOVERNMENT PRINTING OFFICE : 1973--542-650/65

(Continued from inside front cover)

NESS 29 The Operational Processing of Solar Proton Monitor and Flat Plate Radiometer Data. Henry L. Phillips and Louis Rubin, May 1972. (COM-72-10719)

NESS 30 Limits on the Accuracy of Infrared Radiation Measurements of Sea-Surface Temperature From a Satellite. Charles Braun, December 1971. (COM-72-10898)

NESS 31 Publications and Final Reports on Contracts and Grants, 1970--NESS. December 1971. (COM-72-10303)

NESS 32 On Reference Levels for Determining Height Profiles From Satellite-Measured Temperature Profiles. Christopher M. Hayden, December 1971. (COM-72-50393)

NESS 33 Use of Satellite Data in East Coast Snowstorm Forecasting. Frances C. Parmenter, February 1972. (COM-72-10482)

NESS 34 Chromium Dioxide Recording--Its Characteristics and Potential for Telemetry. Florence Nesh, March 1972. (COM-72-10644)

NESS 35 Modified Version of the Improved TIROS Operational Satellite (ITOS D-G). A. Schwalb, April 1972. (COM-72-10547)

NESS 36 A Technique for the Analysis and Forecasting of Tropical Cyclone Intensities From Satellite Pictures. Vernon F. Dvorak, June 1972. (COM-72-10840)

NESS 37 Some Preliminary Results of 1971 Aircraft Microwave Measurements of Ice in the Beaufort Sea. Richard J. DeRycke and Alan E. Strong, June 1972. (COM-72-10847)

NESS 38 Publications and Final Reports on Contracts and Grants, 1971--NESS. June 1972. (COM-72-11115)

NESS 39 Operational Procedures for Estimating Wind Vectors From Geostationary Satellite Data. Michael T. Young, Russell C. Doolittle, and Lee M. Mace, July 1972. (COM-72-10910)

NESS 40 Convective Clouds as Tracers of Air Motion. Lester F. Hubert and Andrew Timchalk, August 1972. (COM-72-11421)

NESS 41 Effect of Orbital Inclination and Spin Axis Attitude on Wind Estimates From Photographs by Geosynchronous Satellites. Linwood F. Whitney, Jr., September 1972. (COM-72-11499)

NESS 42 Evaluation of a Technique for the Analysis and Forecasting of Tropical Cyclone Intensities From Satellite Pictures. Carl O. Erickson, September 1972. (COM-72-11472)

NESS 43 Cloud Motions in Baroclinic Zones. Linwood F. Whitney, Jr., October 1972. (COM-73-10029)

NESS 44 Estimation of Average Daily Rainfall From Satellite Cloud Photographs. Walton A. Follansbee, January 1973. (COM-73-10539)

NESS 45 A Technique for the Analysis and Forecasting of Tropical Cyclone Intensities From Satellite Pictures. (Revision of NESS 36) Vernon F. Dvorak, February 1973. (COM-73-10675)

NESS 46 Publications and Final Reports on Contracts and Grants, 1972--NESS. April 1973.

NESS 47 Stratospheric Photochemistry of Ozone and SST Pollution: An Introduction and Survey of Selected Developments Since 1965. Martin S. Longmire, March 1973. (COM-73-10786)

NESS 48 Review of Satellite Measurements of Albedo and Outgoing Long-Wave Radiation. Arnold Gruber, July 1973.

NESS 49 Operational Processing of Solar Proton Monitor Data. Louis Rubin, Henry L. Phillips, and Stanley R. Brown, August 1973.

NESS 50 An Examination of Tropical Cloud Clusters Using Simultaneously Observed Brightness and High Resolution Infrared Data From Satellites. Arnold Gruber, September 1973.

NESS 51 SKYLAB Earth Resources Experiment Package Experiments in Oceanography and Marine Science. A. L. Grabham and John W. Sherman, III, September 1973.